Heliyon 10 (2024) e26288

Contents lists available at ScienceDirect

Heliyon

journal homepage: www.cell.com/heliyon

Research article

Durability, thermo-physical characteristics, and mechanical strength prediction of green Portland cement matrix incorporating recycled soda-lime glass and lead glass

Tchedele Langollo Yannick [a,b,*], Essomba Essomba Juste Constant [a,b], Emini Pierre Boris Gael [b], Boroh Andre William [b], Mambou Ngueyep Luc Leroy [b], Tchamba Arlin Bruno [a], Ngounouno Ismaïla [b]

[a] Local Materials Promotion Authority (MIPROMALO), Yaounde, Cameroon
[b] School of Geology and Mining Engineering, University of Ngaoundere, Meiganga, Cameroon

ARTICLE INFO

Keywords:
Calcination
Acid attack
Lead glass
Soda-lime glass
Cement

ABSTRACT

The current study is concerned with acid and calcination durability, thermal and thermo-physical properties, and mechanical strength prediction of mortars containing soda-lime glass (PVS) and lead glass (PVP). It demonstrates that up to 30% of PVP (PVP30) and PVS (PVS30) enhancements lessen the consequences of acid attack. In both cases, 20% additions show the best acid resistance at 2 days, but mortars with 10% addition resist better at 28 days. Furthermore, sulfuric acid damages the formed mortars more aggressively than hydrochloric acid. According to the thermal study, the loss of mass owing to calcination is reduced with increasing glass addition. It falls from 22% to −19.5% for PVS30 and -18% for PVP30. The flexural strengths of the calcined mortars significantly drop after firing, although the compressive strengths are higher at 400 °C than at ambient temperature. However, at 600 °C, a 20% glass addition retains the mortar's fire resistance. However, around 800 °C, all formulations mechanically deteriorate. PVP20 has the best fire behavior with relative variations of 48.6% at 400 °C, 18.5% at 600 °C, and −45.8% at 800 °C, while PVS20 has 45.4% at 400 °C, 24.8% at 600 °C, and −33.1% at 800 °C. The hydrates found in the calcined mortars emphasize autoclave reactions that improve mechanical characteristics between 400 and 600 °C, whereas at 800 °C, advanced dehydration of the matrix results in a generalized decrease in resistance. Furthermore, the gradual inclusion of glass reduces the thermal conductivity of mortars correspondingly. The inclusion of 30% PVS results in a reduction of −38.99%, while 30% PVP results in a reduction of −49.95%. The other thermophysical parameters are calculated as a function of these values. The models developed in the area of mechanical strength prediction using the Multilayer Perceptron (MLP) method of Artificial Neural Network (ANN) allow for R^2 correlation coefficients of 0.86–0.92 during training with the database and 0.77 to 0.90 during validation, with values of MAE $\leq$ 2.12 and RMSE $\leq$ 2.67 in all situations.

* Corresponding author. Local Materials Promotion Authority (MIPROMALO), Yaounde, Cameroon.
E-mail address: yannicktl@yahoo.com (T.L. Yannick).

https://doi.org/10.1016/j.heliyon.2024.e26288
Received 17 July 2023; Received in revised form 2 February 2024; Accepted 9 February 2024
Available online 15 February 2024

1. Introduction

After water, concrete is the second most commonly utilized substance on the earth [1]. Its production is mostly determined by the availability of natural resources. Cement is an important component of concrete [2]. More than 2.8 billion tons of cement are produced each year, with this figure anticipated to rise to 4 billion by 2050 [3]. The chemical and thermal combustion processes used in cement manufacture are a significant source of CO_2, accounting for approximately 8% of yearly global CO_2 emissions [4]. According to the report, the total area of buildings in the world in 2016 was approximately 235 billion square meters (m^2), and forecasts indicated that this area is expected to double over the next 40 years, which is equivalent to adding the total area of Japan's buildings to the planet every year until 2060.

Otherwise, glass can be created by melting a mixture of silica (silicon oxide), sodium carbonate, dolomite ($CaMg(CO_3)_2$), and limestone ($CaCO_3$) at high temperatures, up to 1600 °C, and special additives are used to give the glasses their colors and [5]. Depending on the chemical composition and additives used, various types of glass are produced, including vitreous silica, alkali silicates, soda-lime glasses (containers, floats, sheets, light bulbs, and tempered ovenware), borosilicate glasses (chemical, pharmaceutical, and tungsten sealing devices), and lead glasses (color TV funnels, neon tubes, electronic parts, and optically dense flint), and aluminosilicate glasses (combustion tubes, fiberglass, and resistant substrates) [6]. Sheet glass requires 1.73 kg of raw ingredients, 0.15 m^3 of water, and 7–8 GJ/t of energy [7]. The heavy use of energy in these processes results in substantial CO_2 emissions, estimated at 0.57 t/t of glass produced, as well as other greenhouse gases [8]. According to the International Energy Agency (IEA), global glass output was roughly 89.4 million tons in 2007. It increased to 150 million tons in 2014 and continues to rise as industrialization and living conditions improve [9]. Glass is potentially indefinitely recyclable, however only 27 million tons of glass are recycled each year, accounting for 21% of global glass production [10]. This low percentage is attributed by the author to the high expenses of recycling mixed and contaminated glass, which necessitates selective sorting, as well as the risky nature of special glass. The increase in glass production is thus mirrored in the increase in glass waste, which is a concerning issue that must be addressed.

Because of the ever-increasing demand for materials and the capacity to recycle diverse materials [11], the construction sector can give a compelling solution to decreasing the environmental footprint of the cement and glass industries [12]. Glass has the same chemical composition and physical qualities as sand and cement [13]. With this in mind, studies are being done to investigate the use of recycled waste glass as Supplementary Cementing Material (SCM). The findings of this study revealed that finely powdered glass was thought to be pozzolanic [14]; Soda-lime glasses and lead glasses could be used in cementitious matrices [15]; a glass grain size of 75 μm was sufficient to achieve a good pozzolanic activity index [16]; the strength of cementitious matrices with glass addition increased with the content of glass in the mixtures [17,18]; The color of the glass added to the mortar affected its expansion [19]; glass content had a significant impact on the mechanical performance of the matrices [20–22]; Glass powder's pozzolanic activity was low at young ages but increased with age [23–25]; and adding glass improves cement workability [26–29]. While these findings are generally positive, it has been claimed that the strength of mortars and concretes declines as glass content increases [30–32]. Furthermore, various investigations [17,18,33–39] have identified and described the role of the hydrates that emerge in cementitious matrices with the addition of glass. Babé et al. [40] addressed the thermophysical properties of construction materials, which influence the thermal comfort of the structures built, Kowa et al. [41] on Poto-Poto Compressed Blocks, and Mbou et al. [42] on a hybrid composite with polymer matrix with raffia vinifera cork and Bambusa vulgaris. Santiago et al. [43] conducted a literature review on the properties of cementitious matrices amended with glass powder, which revealed that, despite the scarcity of work on the thermal behavior of these matrices, they represented an interesting line of investigation, because numerous mineral additions to the cement had a positive influence on thermal properties. Moreover, cement degradation mechanisms are a developing field of research in the realm of construction materials [44–47]. Previous research has shown that sulfuric acid and hydrochloric acid deteriorate cementitious matrices extensively, producing thaumasite [36,48] and monochloroaluminate at the end of the chain [37,48,49]. In terms of fire-induced degradation, several writers [50,51] claim that the more thermally stable a supplemental cementing material is, the less the cementitious matrices are vulnerable to vapor pressure degradation. New areas of binary binder research have been interested in forecasting their behavior to lower the expense of the work. In this regard, Eskandaria et al. [52] demonstrated that the Artificial Neural Network could predict the compressive strengths of mortars containing sodium chloride with an R^2 of up to 0.999. Apostolopoulou et al. [53] predicted the mechanical behavior of natural hydraulic lime mortars using the same method, with R^2s of 0.9803. Other mathematical methods, such as nonlinear regression [54], or Box–Behnken Optimization Approach [55], were also used to asses cement properties. These studies show that cementitious matrices are amenable to prediction using various approaches. In this regard, the MLP artificial neural network has proven to be quite useful [56–59].

Despite all of the research on glass in cement, its usage as a cement component remains controversial. It is maintained by the research results' conflict, which only more research is likely to resolve. Thus, to better understand the behavior of glass powder as supplementary cementing material, this work proposes to use soda-lime and lead glass powder as supplementary cementing materials, to investigate the acid and calcination strengths of mortars containing these materials, to identify the hydrates formed during calcination and the mechanism by which they form, to assess their thermo-physical behaviors, and finally to determine the effectiveness of the Artificial Neural Network (ANN) Multilayer Perceptron Method (MLP) in predicting the mechanical strengths of these mortars. As a result, it will address issues of durability and thermal comfort of building materials, informing users about reliability and potential energy savings/losses; improving understanding of the reactions of mineral additions in cement; and employing numerical methods in the study of the developed materials.

2. Materials and methods

2.1. Materials

To complete this project, two types of glass were used: soda-lime glass and lead glass. Cathode Ray Tubes (CRT) were gathered from landfills in the city of Yaounde and prepared for use as cementitious additions. These CRT glasses were cleaned, crushed, ground, and sieved to a particle size of around 75 μm, and the resulting samples were dubbed PVP. The chemical composition and mineral analysis are shown in Table 1 and Fig. 1.

The soda-lime glasses used were an equiproportional mixture of three types of packing bottles (clear bottles, green bottles, brown bottles) gathered from domestic garbage, cleaned, pulverized, sieved to a particle size of around 80 μm, and labelled PVS. Table 2 and Fig. 2 reveal the chemical composition and mineral analyses.

Both glass types were added to cement with substitution rates of 10 wt%, 20 wt%, and 30 wt%.

According to the specification [60], the cement used was CPJ-CEM II/A-P 42.5R, manufactured by Dangote Cement Cameroon S.A, based in Douala at Bonaberi, and sold in 50 kg bags. Table 3 illustrates the physicochemical parameters of this cement, and Fig. 3 shows the XRD data. This cement is known as Ordinary Portland Cement (OPC) in the current study.

Finally, the sand used for making the mortar specimens comes from the Sanaga River's banks. To remove tiny particles, it was washed through sieves on an 80 μm screen. This sand was dried in an oven at 105 °C for 24 h before sieving into distinct fractions according to the European Committee of Standardization (CEN) for normal sand. The obtained physicochemical properties, XRD result, and grain size curve are shown in Table 4, Fig. 4, and Fig. 5.

2.2. Methods

2.2.1. Flexural strength test

The flexural strength test is performed on $4 \times 4 \times 16$ cm^3 prismatic specimens following the standard [61], at 2, 7, 28, 56, 90, 150, and 300 days of cure. The specimens are put in turn between the supports of the flexural tester, and the load is applied. The breaking load value is recorded and denoted as "RF." The Flexural strength is given by Equation (1):

$$RF = \frac{1,5 \times F_f \times L}{b^3} \quad (1)$$

With:

RF = Flexural strength in MPa.

L = distance between lower supports in mm.

F_f = maximum breaking load in N.

b = specimen thickness (b = 40 mm).

2.2.2. Compressive strength test

The compressive strength test is performed on $4 \times 4 \times 16$ cm^3 prismatic specimens in line with the standard [61], at 2, 7, 28, 56, 90, 150, and 300 days of cure. The test is carried out on specimen half-prisms obtained following the flexural strength test. Specimen faces in contact with the compression device must be flat and perpendicular to the specimen axis. The specimen faces are then placed on the compression device's platens (Fig. 3), and the load is applied to each specimen. The breaking load is recorded and denoted as "Fc" each time. The compressive strength is determined by Equation (2):

$$RC = \frac{F_c}{S} \quad (2)$$

With:

RC = Compressive strength MPa.

Fc = Maximum breaking load in N.

S = Specimen cross-section in mm^2 (S = 1600 mm^2).

2.2.3. Infrared spectrometry test (FT-IR)

FT-IR is performed on the cement paste by depositing approximately 1 mg of powdered material on the surface of a diamond ATR (Attenuated Total Reflection) crystal. The spectrum is recorded directly after folding back the crank to cover the sample. This research was conducted using a Bruker Alpha-p IR spectrophotometer in transmittance mode with a wavelength range of 4000–400 cm^{-1}. It was carried out in the Faculty of Science's Analytical Chemistry Laboratory at the University of Yaoundé I.

Table 1
XRF of base oxides of PVP sample.

Oxides	SiO_2	Al_2O_3	Fe_2O_3	CaO	MgO	SO_3	K_2O	Na_2O	P_2O_5	LOI
PVP	25.28	1.23	0.15	2.02	0.7	0	6.8	5.68	0	0.7

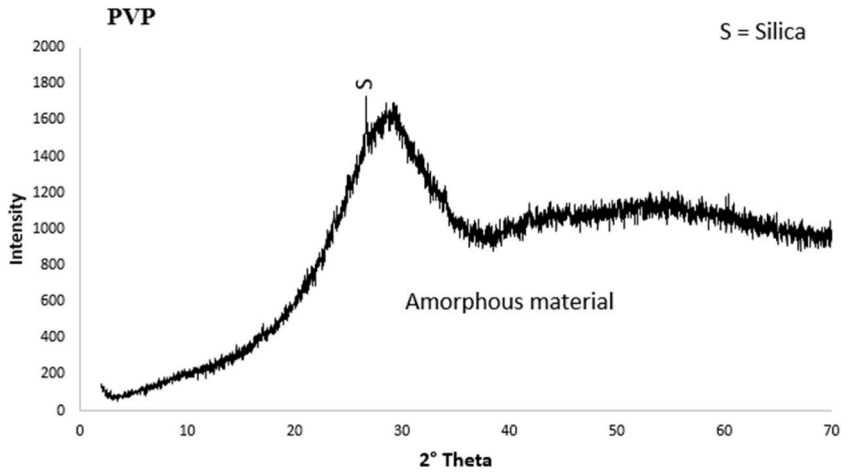

Fig. 1. XRD of CRT glass powder.

Table 2
Chemical composition of soda-lime glass powder.

Oxides	SiO_2	Al_2O_3	Fe_2O_3	CaO	MgO	Na_2O	K_2O	TiO_2	BaO	Cr_2O_3	SO_3	LOI
PVS	72.25	1.03	0.07	10.94	1.28	13.83	0.04	0.13	0.19	0.07	0.16	0.6

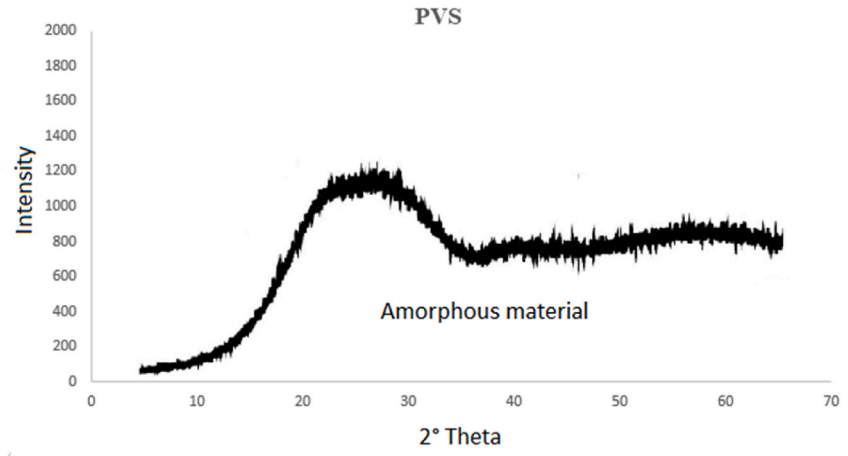

Fig. 2. XRD result of soda-lime glass powder.

2.2.4. Thermogravimetric analysis (TGA)

Thermal breakdown, evaporation, reduction, desorption, sublimation, oxidation, absorption, and other processes can all be observed with TGA. It can also be used to assess compound thermal stability, estimate the temperatures at which chemical reactions occur, and measure specific volatile chemicals in a solid sample. The cement paste were analyzed at the University of Hanover, Germany, using a standard-compliant apparatus (model DTA409 PC/PG, NETZSCH, Germany) that circulates Helium as a sweep gas at a flow rate of 60 mL/min and an average temperature rise of 10 °C/min.

2.2.5. X-ray diffractometry

The XRD was carried out on the cement paste following the protocol of the University of Liège's Geology and Sedimentary Environment Laboratory (AGES). The data were collected using a Brucker D8-Advance diffractometer with copper Kα1 radiation ($\lambda =$ 1.5418 Å). The goniometer measurement speed is 10 s per step, and the rotation speed is 2°2θ per minute, resulting in an analysis time of several minutes to cover an angular range of $2\theta = 2$–$70°$ for non-oriented powders and $2\theta = 2$–$30°$ for oriented slides. The acceleration voltage is 40 KV, and the current is 30 mA. It is linked to a computer for automatic data collection. DIFFRAC Plus Release 2000-EVA 6.0, the software used for crystal phase identification, and the data presented in the PDF files (Powder Diffraction File) are

Table 3
Physico-chemical characteristics of cement.

Cement	SiO_2	Al_2O_3	Fe_2O_3	CaO	MgO	SO_3	K_2O	Na_2O	P_2O_5	LOI	Rejection at 0.08 mm (%)	Bulk density (g/cm^3)	Specific weight (g/cm^3)	SSB (cm^2/g)
OPC	18.68	5	3.31	62.88	1.04	3.78	0.36	0.35	0.11	5.94	0.59	0.91	2.98	3353

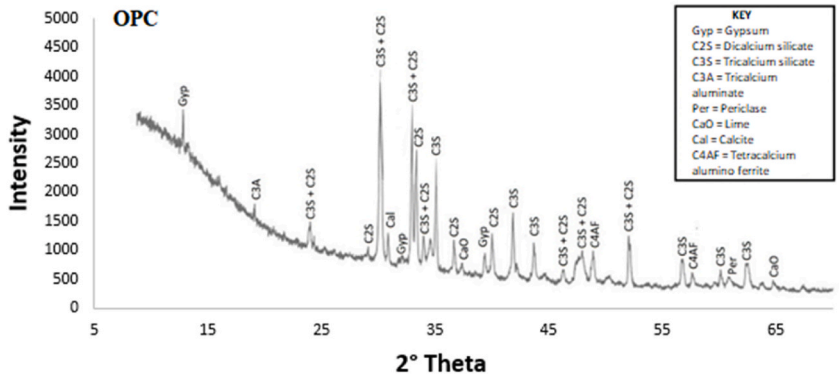

Fig. 3. XRD results on CPJ CEM II/A-P 42.5 cement (OPC).

Table 4
Physico-chemical characteristics of the treated sand.

Physical properties				Chemical properties									
Absolute density (g/cm3)	Bulk density (g/cm3)	Fineness modulus	Sand equivalent (%)	SiO_2	Al_2O_3	Fe_2O_3	CaO	MgO	SO_3	K_2O	Na_2O	P_2O_5	LOI
2.68	1.49	2.89	99.6	63.19	5.83	3.18	2.02	0.33	0.05	2.52	0.69	0.06	1.55

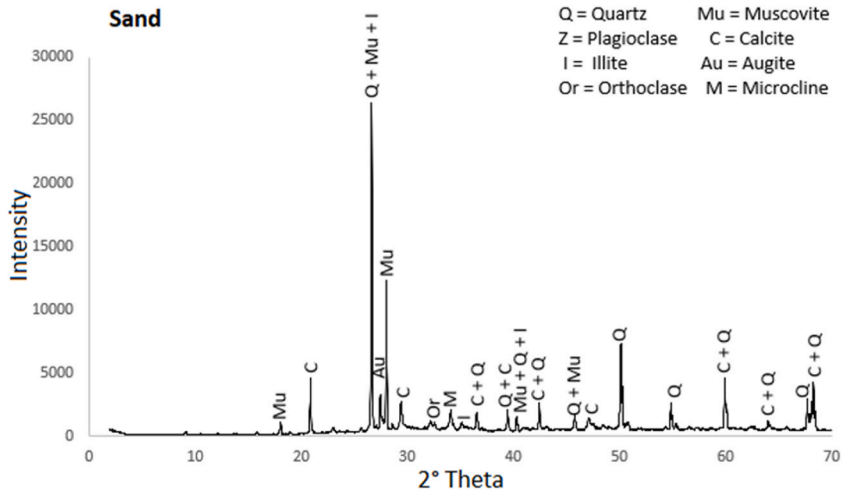

Fig. 4. XRD result of Sanaga sand.

utilized to evaluate the diffractograms obtained.

2.2.6. *Fire test of mortar specimens*

After 28 days of curing, the fire test is performed following the standard [62], at three temperatures (400 °C, 600 °C, and 800 °C) to evaluate the loss of mortar strength due to fire action. Mortars are prepared following the various formulations defined for the study, followed by wet curing and drying at 105 °C for 24 h, calcination at various temperatures, and finally flexural and compressive strength tests.

2.2.7. *Acid durability test: measuring mass loss*

The standard-compliant durability test [63], involves evaluating the mass loss caused by immersing test specimens in 5% concentrated acid. It allows us to investigate the degradation mechanisms of cementitious matrices in the face of the external acid attack that occurs gradually after they have been used in the construction of a structure. To perform this test, mortar specimens are prepared and placed in water for 28 days to mature. They are then removed from the oven, dried for 48 h, and weighed (M_0). They are then immersed in sulfuric acid on one side and hydrochloric acid on the other, and after 2, 7, and 28 days, they are extracted,

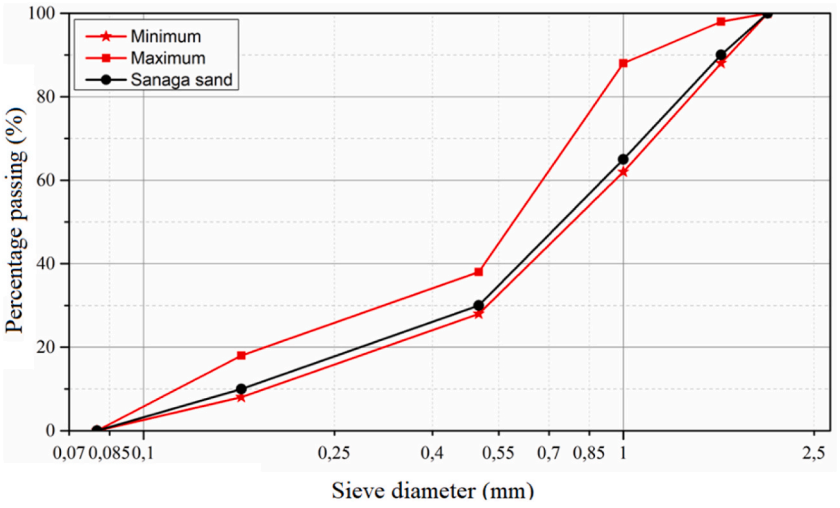

Fig. 5. Grading curve of standardized sand according to CEN.

oven-dried for 48 h, and weighed (M_i). Equation (3) determines mass loss during acid attacks:

$$M_{Pi} = \frac{M_i - M_0}{M_0} \times 100 \quad (3)$$

With:

M_{Pi} = Mass loss at i days in %;
M_0 = Initial mass in g;
M_i = Mass at i days in g.

2.2.8. Specimen preparation for thermo-physical properties estimation

The mortar specimens used to estimate thermo-physical properties were made using 10 × 10 × 4 cm^3 steel molds. They are formulated with the same proportions of materials as the previous mortars. The quantities used to make 03 specimens per formulation are given in Table 5.

2.2.9. Measurement of thermo-physical properties

Conductivity, effusivity, diffusivity, and heat capacity are the thermo-physical qualities investigated. The asymmetric hot-plane approach is used to measure these thermophysical characteristics. Several researchers have employed this strategy successfully, including [40–42]. It was designed primarily to assess the thermal characteristics of "heavy" building materials with thermal conductivities ranging from 0.2 to 5 W m^{-1} K^{-1} (earth-based materials, mortars, concretes, wood, plastics, and so on). The experimental set-up used for the measurement (Fig. 6) is available at the L3E Laboratory of the National Advanced School of Engineering of Yaounde.

The test involves sandwiching a thin, flat heating element with the same surface area (10 × 10 cm^2) as the sample between it and a polystyrene foam sample. A thermocouple made of two wires with diameters less than or equal to 0.05 mm is glued to the face of the element that comes into contact with the polystyrene. A polystyrene block is placed on top of the sample, and the whole thing is sandwiched between two 4 cm thick aluminum blocks. A flux step is applied to the heating element, and the thermocouple's temperature change T(t) is recorded. The presence of the thermocouple generates no additional contact resistance because it is in touch with a deformable material. Furthermore, because polystyrene is an insulator, the contact resistance between the heating element and the polystyrene is insignificant. The temperatures T(t) obtained are processed using Excel software, assuming that heat flow at the center of the heating element is unidirectional.

Thermal effusivity is determined using the full model, using the thermal effusivity value pre-estimated from the simple model with experimental temperature readings as the beginning value. The Levenberg-Marquardt algorithm [64] is a mathematical algorithm.

Table 5
Materials used to make mortar samples.

Glass powder content (%)	Mass of cement (g)	Mass of glass powder (g)	standardized sand (g)	Mass of water (g)
0	500	0	1350	225
10	450	50	1350	225
20	400	100	1350	225
30	350	150	1350	225

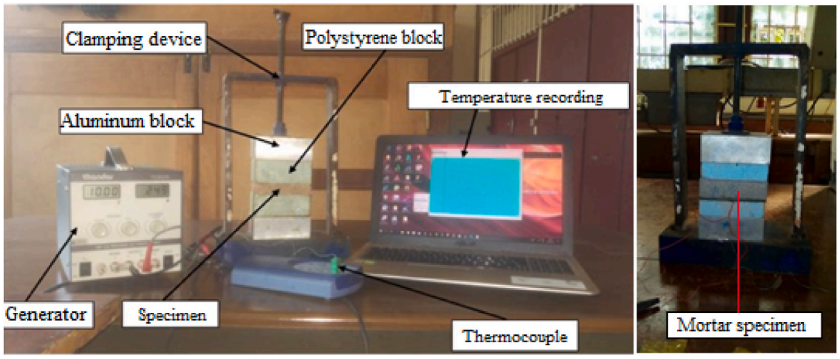

Fig. 6. The experimental hot plate device.

Integrated within the Matlab code is used to estimate the value of E that minimizes the total of the squared deviations $\psi = \sum_{i=1}^{n}[\Delta T_{exp}(t_i) - T_{model}(t_i)]^2$ between the experimental and theoretical curves $\Delta T_{exp}(t) = T(0,t) - T_a$. The estimation was performed over a time interval [t_0, tmax] so that the residuals are centered around zero degrees, allowing the model to be validated. Three measures of each mixture of mortar specimens are tested and the mean values are retained. The estimation of effusivity (E) and thermal capacity $\rho c = (\rho c)_{exp}$ is done for four varied content of the glass. The thermal conductivity and thermal diffusivity are respectively obtained by Equations (4) and (5):

$$\lambda = \frac{E^2}{\rho c} \tag{4}$$

$$a = \frac{\lambda}{\rho c} \tag{5}$$

With:

a = Thermal diffusivity expressed in m^2s^{-1}
E = Effusivity expressed in $J/k.m^2.S^{1/2}$
λ = Thermal conductivity expressed in $W.m^{-1}.K^{-1}$
c = Heat capacity expressed in $J.K^{-1}$.

2.2.10. Prediction using MLP method of the artificial neural network

In each case, a set of 56 physicomechanical data for mortars with additional soda-lime glass and lead glass were utilized to estimate mechanical strengths using the Artificial Neural Network (ANN) Multilayer Perceptron Method (MLP). Table 6 lists the hyper-parameters defined for predicting flexural strength (RF-PVP, RF-PVS) and compressive strength (RC-PVP, RC-PVS) of mortars with additional PVP and PVS.

A hyperparameter search algorithm is used to discover the optimal parameters, i.e. the parameters that provide the best predictions [65,66]. The complete approach was created in a Python program that ran on the PyCharm Community Edition 2021.2.3 platform.

The following factors are used to assess the accuracy of prediction results:

- The coefficient of determination (R^2) is provided by Equation (6):

$$R^2 = \frac{SSR}{SST} = \frac{\sum_{i=1}^{n}(\widehat{X}_i - \overline{X})^2}{\sum_{i=1}^{n}(X_i - \overline{X})^2} \tag{6}$$

Table 6
MLP hyperparameters for mechanical strength prediction.

Hyperparameters definition	
Learning rate	[0.0001, 0.5]
Number of hidden layers	[1,10]
Neurons per layer	[1, 300]
Batch size	[8, 16, 32, 64, 128, 256]
Activation function	['tanh', 'sigmoid', 'relu']
Optimizer	['adam', 'rms', 'sgd']

- The mean absolute error (MAE) is given by Equation (7):

$$MAE = \frac{1}{N}\sum_{i=1}^{N}|X_i - P_i| \tag{7}$$

- The root-mean-square error (RMSE) is given by Equation (8):

$$RMSE = \sqrt{\frac{\sum_{i=1}^{N}(X_i - P_i)^2}{N}} \tag{8}$$

With:

X_i which represents the ith experimental value, $\widehat{X}_i$ the ith predicted value and $\overline{X}$ the mean;
P_i represents the ith predicted value;
N represents the number of data points.

3. Results and discussion

3.1. Durability of mortars with glass powder addition

3.1.1. Durability against acid attack

The resistance of mortars to acid attack is determined here by studying the mass loss of mortars immersed in acids (H_2SO_4 and HCl) concentrated at 5% following the standard [63]. To visually determine the effect of these acids, images of the samples were taken after 2 days of curing in 20% concentrated sulfuric acid (Fig. 7(a)) and 5% concentrated hydrochloric acid (Fig. 7(b)) following the standard.

These images show that at 20% acid concentration, the control mortar sample (OPC) is more attacked than the matrices with glass addition, and the higher the percentage of addition, the less attacked the material appears. Under standard conditions, i.e. at 5% concentration, mortars remain coherent despite acid-induced corrosion and can therefore be tested. The results of mass loss tests under these conditions are shown in Fig. 8.

The results show mass losses for mortars with added PVP ranging from −3.06% to −2.44% in HCl and from −3.45% to −2.61% in H_2SO_4, at 2 days curing. At 7 days, they vary from −5.07% to −3.61% in HCl and from −8.42% to −6.37% in H_2SO_4; at 28 days, they increase from −12.58% to −8.00% in HCl and from −16.77% to −12.66% in H_2SO_4. Similarly, mass losses of mortars with added PVS vary at 2 days from −3.06% to −2.40% in HCl and from −3.45% to −2.57% in H_2SO_4; at 7 days from −5.07% to −4.40% in HCl and from −8.42% to −6.96% in H_2SO_4; at 28 days from −12.58% to −9.48% in HCl and from −16.77% to −13.57% in H_2SO_4. As a result, the acid attack on these mortars becomes more severe over time. Sulfuric acid has a stronger impact on the matrices than hydrochloric acid and cementitious admixtures aid to decrease the impact of this attack. At a young age (2 days), additions of 20% PVP and PVS provide the best acid resistance, whereas, at an older age (28 days), where the degree of hydration is greater, mortars with 10% addition withstand acids better.

It is necessary to examine the attack mechanisms to comprehend the outcomes achieved. Following this reasoning, hydrochloric acid targets cementitious matrices by forming $CaCl_2$ salts through reactions with Portlandite, calcite, and CSH. In turn, this product interacts with tricalcium aluminate to generate monochloroaluminate. The reaction Equations (9)–(12) are as follows [37,48,49]:

$$Ca(OH)_2 + 2HCl \leftrightarrow CaCl_2 + 2H_2O \tag{9}$$

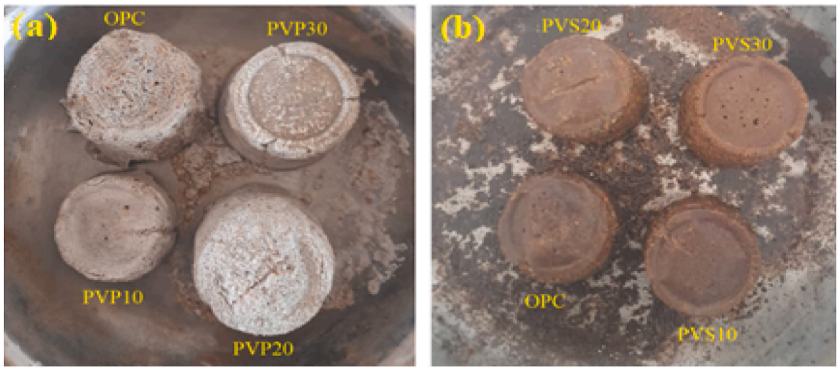

Fig. 7. The image of (a) 20% sulfuric acid attack on mortar samples with PVP addition and (b) hydrochloric acid attack on mortar samples with PVS addition.

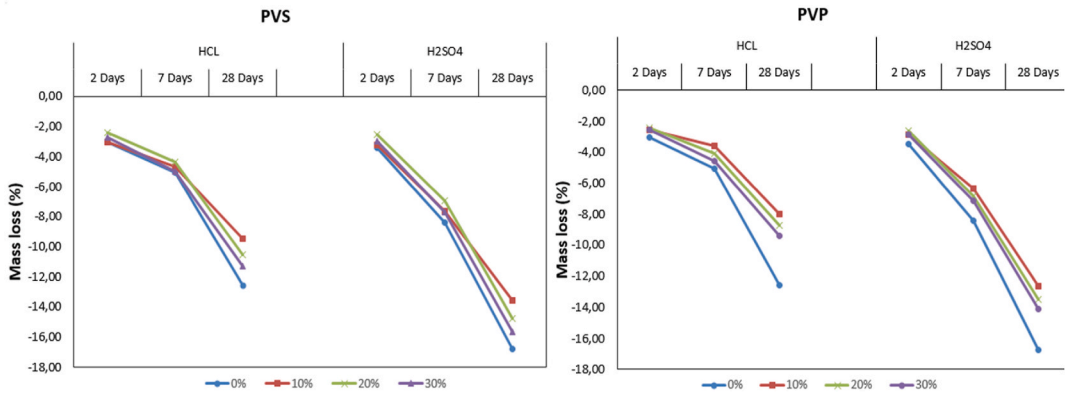

Fig. 8. Mass loss results for mortar samples with added PVS and PVP attacked with hydrochloric acid and sulfuric acid.

$$CaCO_3 + 2HCl \rightarrow CaCl_2 + CO_2 + H_2O \tag{10}$$

$$CaO{\cdot}2SiO_2{\cdot}3H_2O + 2HCl \leftrightarrow CaCl_2 + 2(SiO_2{\cdot}H_2O) + 2OH^- \tag{11}$$

$$3CaO \cdot Al_2O_3 + CaCl_2 + 10H_2O \longleftrightarrow \underset{\text{Monochloroaluminate (AFm)}}{3CaO \cdot Al_2O_3 \cdot CaCl_2 \cdot 10H_2O} \tag{12}$$

Sulfuric acid reacts with Portlandite to form gypsum. Gypsum then enters a chain reaction to form monosulfate, secondary ettringite, and finally thaumasite [36,48]. The reaction equations are given by Equations (13)–(17):

$$Ca(OH)_2 + H_2SO_4 \rightarrow CaSO_4{\cdot}2H_2O \tag{13}$$

$$\underset{\text{Tricalcium Aluminate}}{3CaO.Al_2O_3} + \underset{\text{gypsum}}{3CaSO_4 \cdot 2H_2O} + \underset{\text{water}}{26H_2O} \rightarrow \underset{\text{ettringite}}{Ca_6Al_2(SO_4)_3(OH)_{12}.26H_2O} \tag{14}$$

$$\underset{\text{Ettringite}}{Ca_6Al_2(SO_4)_3(OH)_{12}.26H_2O} + \underset{\text{tricalcium aluminate}}{2(3CaO.Al_2O_3)} + \underset{\text{water}}{4H_2O} \rightarrow \underset{\text{monosulfate}}{CaO.Al_2O_3.CaSO_4.12H_2O} \tag{15}$$

$$\underset{\text{Monosulfoamuninate (AFm)}}{3CaO \cdot Al_2O_3(CaSO_4) \cdot 12H_2O} + \underset{\text{Anhydrite}}{2CaSO_4} + \underset{\text{Water}}{20H_2O} \rightarrow \underset{\text{Secondary ettringite (AFt)}}{3CaO \cdot Al_2O_3 \cdot 3(CaSO_4) \cdot 32H_2O} \tag{16}$$

$$\underset{\text{Thaumasite}}{3CaO \cdot Al_2O_3 \cdot 3CaSO_4 \cdot 32H_2O} + 3CaO \cdot 2SiO_2 \cdot 3H2O + 6CaCO_3 + 12H_2O \rightarrow 2CaSiO_3 \cdot CaSO_4 \cdot CaCO_3 \cdot 15H_2O + 6Ca(OH)_2 + 3Al(OH)_3 \tag{17}$$

The incorporation of pozzolanic additives (such as glass powder) into cementitious matrices reduces capillary holes by producing new CSH gels with Portlandite consumption [60]. As acids diffuse less inside the matrix and less Portlandite is available to react, this reaction results in a reduced mass loss [67]. Dinakar et al. [68] go even farther, attributing the minor decrease in the mass of formulations with the lowest strengths to Portlandite's scarcity. Acid attack diminishes as cement content decreases because the glass used as a replacement is chemically inert to many acids, which cement is not [69]. In the same vein, the filler effect of glass will also prevent the diffusion of acid and thus reduce its attack. According to Torri and Kawamura [70], increasing cement fineness accelerates the kinetics of the pozzolanic reaction of mineral admixtures and, as a result, cementitious matrices become less acid sensitive.

According to Rahman and Ojovan [36], a high calcite concentration increases HCl's aggressiveness because the CO_2 produced by reaction (10) is likely to breakdown CSH according to Equation (18):

$$\underset{\text{CSH}}{3CaO \cdot 2SiO_2 \cdot 3H_2O} + 3CO_2 \rightarrow \underset{\text{Monocarbonate}}{3CaCO_3 \cdot 2SiO_2 \cdot 3H_2O} \tag{18}$$

Except in this situation, H_2SO_4 is more aggressive than HCl on Portland cement [48,67]. The work of Siad et al. [71] demonstrated that when mortars with up to 45% glass powder addition were attacked with sulfuric acid, the control sample (OPC) suffered the greatest mass losses. According to Wang [72], these losses decreased steadily with the addition of glass from 0% (OPC) to 50%, with a 10% addition optimum reducing losses.

According to Zivica and Bajza [48], the principal products of sulfuric acid attack reactions are gypsum and ettringite, and these two compounds are often connected with expansion, cracking, and spalling [71]. According to Bertolini et al. [73], this loss of mass would be primarily attributable to the consumption of Portlandite and thus to mass loss. According to Bassuoni et al. [74], H_2SO_4 does degrade CSHs, but only conventional CSHs are impacted, with second-generation CSHs being less damaged; this would explain why

H_2SO_4 attack on OPC causes the biggest mass losses. The inclusion of glass in Portland cement, which has been demonstrated to improve durability against acid attacks, offers an incentive to examine the thermal durability of these matrices as well.

3.1.2. Thermal stability

3.1.2.1. Thermogravimetric investigation. To investigate the effect of the glass additions on the mass loss of calcined matrices and the transformations that occur during calcination, thermogravimetric analysis was performed on cement paste samples with soda-lime glass addition (Fig. 9) and lead glass addition (Fig. 10).

When soda-lime glass powder is added to cement paste, the mass loss for OPC is −22%, −21.5% for PVS10, -20.5% for PVS20, and -19.5% for PVS30 (Fig. 9). When lead glass powder is added, PVP10 loses −19% of its mass, PVP20 loses −18.5%, and PVP30 loses −18% (Fig. 10). These findings indicate that glass powder reduces the mass loss of calcined pulp samples, with lead glass powder showing the least loss. This could be because glass has a smaller loss on ignition than cement, and lead glass's semi-crystalline form makes it less sensitive to fire than soda-lime glass. To better comprehend these losses, the derivative curve depicts the various stages of cement paste dehydration as peaks. As an example:

- The peak between 50 °C and 200 °C corresponds to several phenomena, including Ettringite decomposition generally observed between 50 and 150 °C (Equation (19)) [75,76], water evaporation which takes place between 100 and 130 °C [77], gypsum decomposition at 120–200 °C (Equation (20)) [78,79], and dehydration of CSH gels in the paste at 160–185 °C [77];

$$\underset{\text{Ettringite}}{Ca_6\left[Al(OH)_6\right]_2\cdot(SO_4)_3\cdot 26H_2O} \rightarrow \underset{\text{Monosulfate}}{Ca_4\left[Al(OH)_6\right]_2SO_4\cdot 8H_2O} + \underset{\text{Hemihydrate}}{2CaSO_4\cdot 0.5H_2O} + 17H_2O \quad (19)$$

$$CaSO_4\cdot 2H_2O \xrightarrow[120°C]{} 2CaSO_4\cdot 0,5H_2O \xrightarrow[200°C]{} \underset{\text{Anhydrite}}{2CaSO_4} \quad (20)$$

- The peak between 400 °C and 475 °C corresponds to the dehydroxylation of Portlandite (Equation (21));

$$Ca(OH)_2\ (s) \xrightarrow[Calcination]{} CaO\ (s) + H_2O\ (g) \quad (21)$$

- The peak between 600 °C and 700 °C corresponds to the decarbonation of calcite (Equation (22)) [29,80].

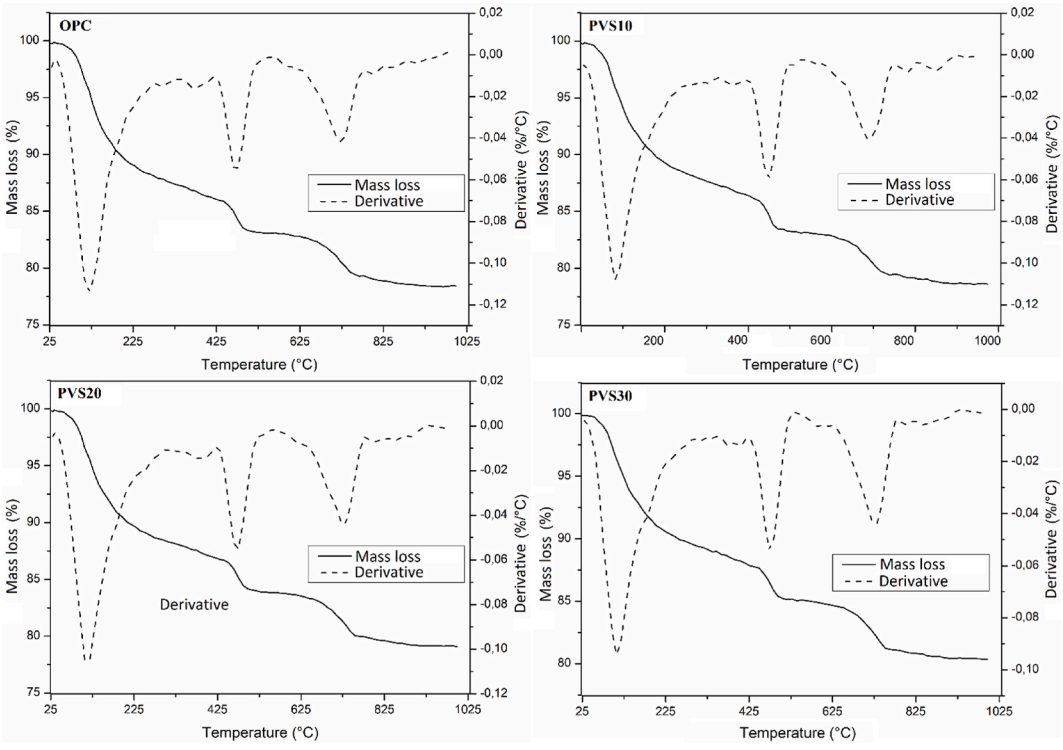

Fig. 9. TGA results on OPC, PVS10, PVS20 and PVS30 mortar samples after 28 curing days.

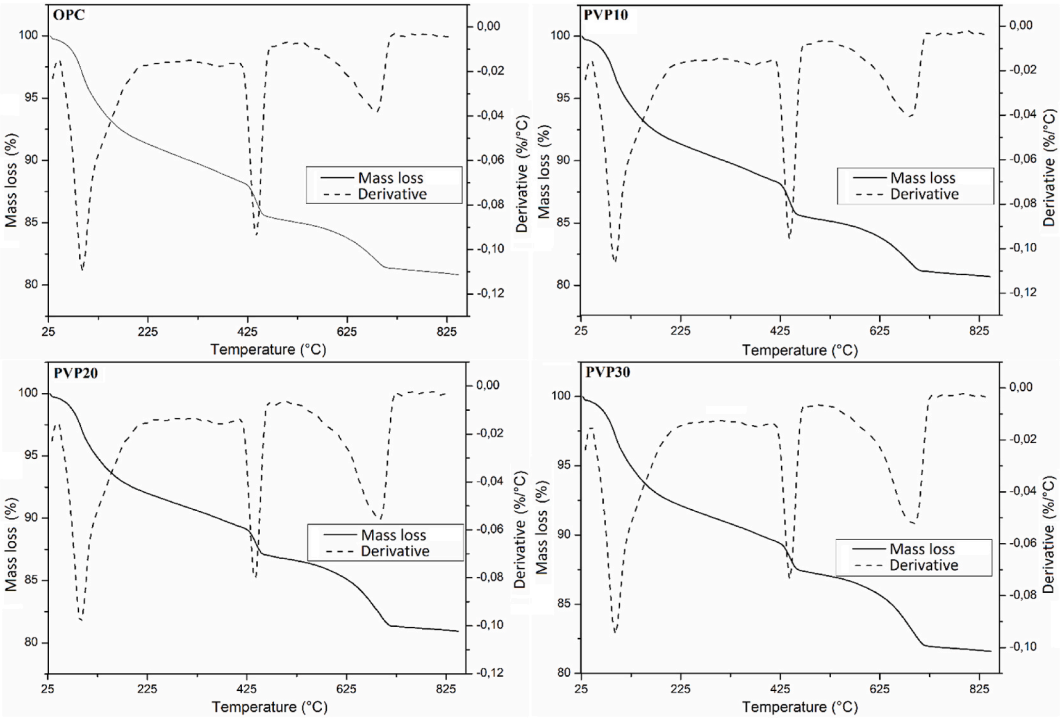

Fig. 10. TGA results on OPC, PVP10, PVP20, and PVP30 mortar samples after 28 curing days.

$$CaCO_3\ (s) \xrightarrow[Calcination]{} CaO\ (s) + CO_2\ (g) \tag{22}$$

The loss of mass caused by Portlandite dehydroxylation is less pronounced in cementitious matrices including glass, and it can be explained by three (03) possible explanations. The first is a decrease in cement quantity, which reduces the amount of Portlandite produced during hydration; the second is the consumption of Portlandite produced by the second-generation pozzolanic reaction; and

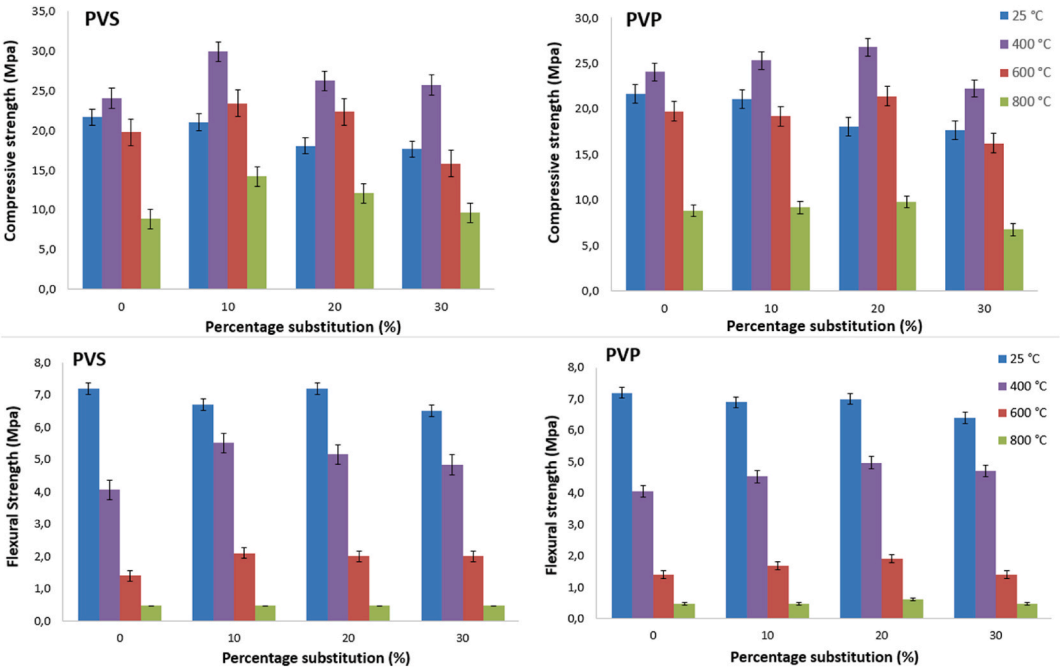

Fig. 11. Results of flexural and compressive strengths of mortars with added PVS and PVP calcined at 400, 600, and 800 °C.

the third is the fineness of the cement additive, which impedes contact between cement grains and slows hydration. This latter explanation explains why mass loss is smaller in matrices with added PVP (Ø < 75 μm) than in those with added PVS (Ø < 80 μm).

In the same vein, Liu et al. [29] report that adding recycled glass to mortars reduces mass loss of high-strength samples throughout the thermogravimetric analysis. After calcination at 1000 °C, the remaining mass of the control sample was around 83.75%, which was the lowest compared to 84.08%, 85.26%, and 87.59% obtained for samples containing 10%, 30%, and 60% recycled waste glass, respectively. They also ascribe these findings to the fact that recycled glass, by its pozzolanic activity, decreases the proportion of physically bonded water and calcium hydroxide. These findings were supported by Mounanga et al. [81], analytical calculation of Portlandite content, which revealed that for a high glass content (60%), the amount of Portlandite in cementitious matrices decreased significantly after 90 days of curing, with −46.32% for high-strength samples and −52.4% for normal-strength samples. The main benefits of incorporating glass into cementitious matrices appears to be well known, and it might be confirmed by investigating the mechanical properties of calcined mortars.

3.1.2.2. Mechanical properties of mortars with added glass at 400 °C, 600 °C and 800 °C. Based on the favorable thermogravimetric results, the fire resistance of PVP and PVS mortars was tested by examining their flexural strength and compressive strength. Fig. 11 depicts the results.

At 400 °C, compression test results for specimens with additional PVS range from OPC (24 MPa) to PVS30 (25.7 MPa), with PVP10 (29.9 MPa) being the best. PVP additions increase from OPC to PVP20 (26.8 MPa), the optimum, and then fall to PVP30 (22.2 MPa). At 600 °C, the compressive strengths of mortars containing PVS increase from OPC (19.7 MPa) to PVS20 (22.3 MPa), then decrease to PVS30 (15.8 MPa). Except for PVP20 (21.3 MPa), the strengths of mortars with PVP added drop. In terms of compressive strength at 800 °C, the addition of glass powder strengthens mortars up to PVS20 (9.8 MPa) and PVP30 (9.6 MPa) as compared to OPC (8.8 MPa).

Flexural strength is improved by the various glass additives utilized during 400 °C calcination. At 600 °C, the addition of PVP10, PVP20, PVS10, PVS20, and PVS30 improves flexural strengths, however, at 800 °C, the strengths are generally equal to those of the control sample. As a result, the mechanical strengths of mortars containing glass exhibit generally positive calcination behavior. To better illustrate this point, Table 7 shows the variations in mechanical strength between calcined mortars and mortars at room temperature.

These findings suggest that adding glass to mortars between 400 and 600 °C boosts compressive strength significantly. Particularly for 10–30% calcined PVP and PVS addition at 400 °C, 20% PVP addition, and 10–20% calcined PVS addition at 600 °C. This does not apply to flexural strength, which diminishes consistently following calcination.

Similar results were obtained by Salim and Mosaberpanah [82], when a binary mixture of hollow ceramic microspheres (cenospheres) and glass powder were added to mortars calcined at 200, 400, and 600 °C. They obtained small improvements in strength at 200 °C and greater increases at 400 °C, with strength increases of 21.15% and 27.3% for 10% and 20% glass addition, respectively. They also found a decrease in the strength of certain combinations at 600 °C. According to Seleem et al. [83], the observed variations can be explained as follows:

- At 400 °C, the evaporation process speeds up, creating friction between the mortar layers and necessitating more force to break the specimen. The transport of evaporated water inside the matrix enhances the rate of hydration, resulting in the creation of additional CSH, which increases strength. The binders are additionally autoclaved at 400 °C, which improves hydration, the second-generation pozzolanic reaction, and specimen strength.
- Between 600 °C and 800 °C, dehydration of cement hydrates accelerates, reducing strength. The production of huge vapor pressure, which causes cracks in the mortar, reduces compressive strength.

Glass's poor thermal conductivity relative to cement [38], also plays a significant role in mortar by minimizing calcination deterioration. In this regard, Ibrahim et al. [50] contend that the more thermally stable an addition, the less cementitious matrices

Table 7
Variation in flexural and compressive strengths of calcined mortars with the addition of PVS and PVP compared to the same mortars at room temperature.

Substitution content (%)	Variation in compressive strength of calcined mortars compared to the mortars at room temperature: the case of PVP			Variation in compressive strength of calcined mortars compared to the mortars at room temperature: the case of PVS		
	400 °C	600 °C	800 °C	400 °C	600 °C	800 °C
0	11.1	−8.8	−59.3	11.1	−8.8	−59.3
10	20.4	−8.7	−56.5	42.3	11.3	−32.5
20	48.6	18.5	−45.8	45.4	23.8	−33.1
30	26.2	−7.9	−61.9	45.8	−10.3	−45.5
	Variation in flexural strength of calcined mortars compared to the mortars at room temperature: the case of PVP			Variation in flexural strength of calcined mortars compared to the mortars at room temperature: the case of PVS		
0	−43.6	−80.6	−93.5	−43.6	−80.6	−93.5
10	−34.3	−75.4	−93.2	−20.1	−69.6	−93.2
20	−29.0	−72.6	−91.1	−26.3	−71.4	−93.3
30	−26.4	−78.0	−92.7	−24.3	−68.8	−92.7

experience vapor pressure deterioration. As result, glass improves the cement paste quality by reducing heat transfer inside the matrix and producing a substantial amount of second-generation CSH during the autoclave process. This is why mortars with the best mechanical properties at room temperature presenting good hydration (PVS) are more resistant to calcination up to 800 °C.

3.1.3. Chemical and mineralogical properties at 400 °C, 600 °C and 800 °C

3.1.3.1. Chemical properties: infrared (IR) spectrometry. After 28 days of curing, Infrared Spectrometry analysis was performed on cement pastes with additional PVS and PVP, calcined at 400, 600, and 800 °C, intending to detect chemical species remaining present in the matrix after calcination and likely to explain the mechanical results observed. Fig. 12 depicts IR spectra.

The asymmetric stretching vibration of the O-H bond of free water and the bending stretching of the O-H bond of the water molecules present in gypsum are highlighted by the peak at 3750 cm^{-1} and the bands between 1640 and 1650 cm^{-1}, respectively [84]. Meanwhile, the bands about 3640 cm^{-1} correspond to the vibration of the O-H bond in Portlandite [85]. When compared to the results on raw cement of [86], the low intensities observed reflect practically complete gypsum decomposition and dehydroxylation of Portlandite, which seems more important at 800 °C, as demonstrated by thermal analysis (ATG). At 400 °C, adding glass powder to the paste in amounts ranging from 0% (OPC400) to 30% (PVP30400 and PVS30400) decreases the intensity of Portlandite peaks caused by the second-generation pozzolanic reaction. Despite the use of glass, Portlandite peaks appear to grow at 600 °C. Tantawy [87], attributes this expansion to lime rehydration. These peaks tend to diminish at 800 °C and follow the same pattern as at 400 °C.

Carbonates ($C O_3^{2-}$) characteristic of calcite, generated by the interaction between ambient CO^2 and Portlandite, are assigned to the bands around 2100 cm^{-1}, 1414 cm^{-1}, 872 cm^{-1}, and 712 cm^{-1} [88]. Calcite content is higher at 400 °C than at 600 and 800 °C because, as previously stated, the decarbonation process begins above 600 °C. For all calcination temperatures studied, the intensity of calcite banding rises with the addition of glass to the paste. As a result, glass could improve the resistance of cementitious matrices against hydrate decomposition. Ettringite is represented by the peaks at 1089 cm^{-1} characteristic of the ($S O_4^{2-}$) radical of the sulfate group, which emerges at 600 and 800 °C [89]. Its presence implies that secondary ettringite is likely to form over 600 °C as a result of anhydrite-monosulfate interaction. This is more apparent in OPC600 and OPC800 matrices than in glass-added matrices. The inclusion of soda-lime glass powder appears to be more successful than the addition of lead glass powder in inhibiting this reaction.

Spectral intensity variations between 900 and 1100 cm^{-1} that are neither associated with water nor sulfates refer to the asymmetric stretching vibration in the Si-O subsystem that some works refer to alite (C_3S) [86,90]. For Tantawy [87], the absorption band of 400–520 cm^{-1}, corresponds to the vibration of the (O-Si-O) bond of belite. At 800 °C, the absorption bands of C_3S and C_2S are more intense than at 400 °C. This is due to CSH breakdown into C_2S and C_3S, which begins at 160 °C and worsens with increasing temperature. These intensities rise with the addition of glass due to the increased amount of CSH created by pozzolanic processes, which, once anhydrous due to temperature, add to the pre-existing silicates [91].

It, therefore, appears that the calcination of cementitious matrices provokes reactions that modify the composition of hydrated cement. While chemical analysis has revealed some of these, mineralogical analysis is likely to provide additional information.

3.1.3.2. Mineralogical properties: X-ray diffractometry (XRD). X-ray diffractometry was carried out in addition to IR on OPC, PVS10, PVS20, PVS30, PVP10, PVP20, and PVP30 samples, after 28 days of curing, to distinguish the minerals present in the formulations after calcination at 400, 600, and 800 °C. The results are shown in Fig. 13.

The diffractograms produced allow the identification of hydrates and anhydrous cement compounds. Anhydrous compounds include the classic C_2S, C_3S, C_4AF, C_3A, and CaO [29,92–94]. Hydrates include CSH, Ettringite, Portlandite, Stratlingite, Calcite,

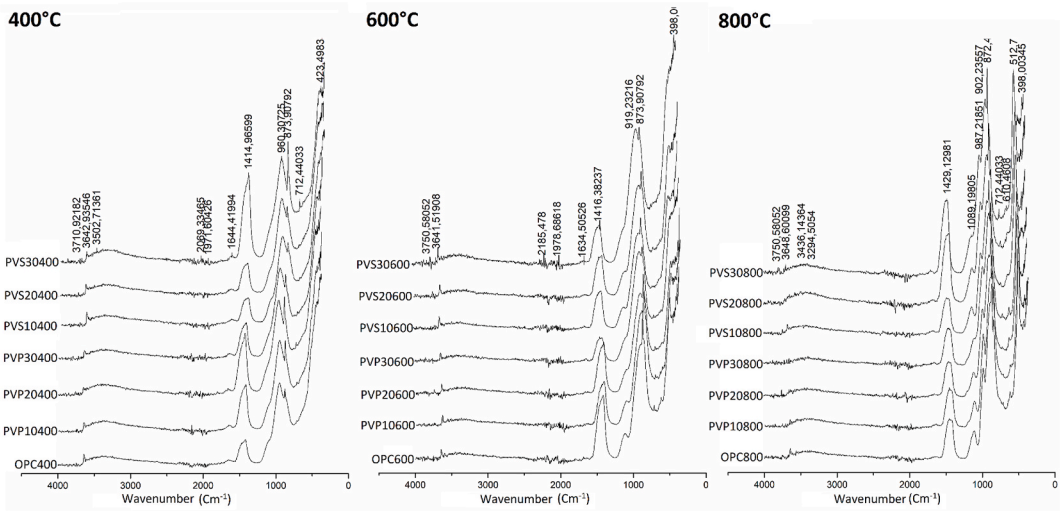

Fig. 12. IR results on cement pastes with added PVS and PVP calcined at 400, 600 and 800 °C.

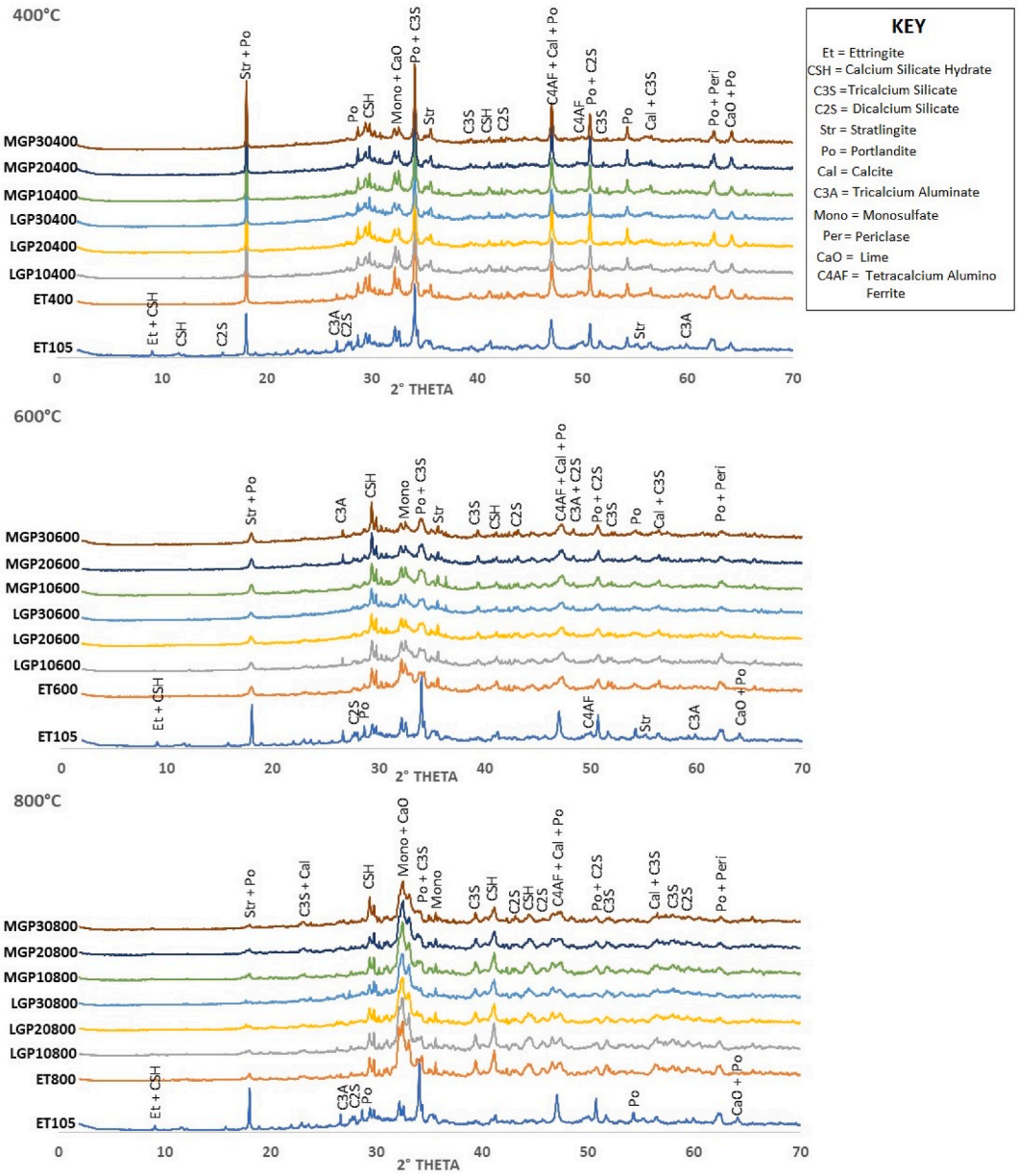

Fig. 13. XRD results on cement pastes with added PVS and PVP calcined at 400, 600, and 800 °C.

Monosulfate, and Periclase [39,95]. The Porlandite peaks of the different formulations grow at 400 °C in comparison to those at 25 °C, with the largest growth observed at 20% glass addition. Some pre-existing peaks of C_2S, C_3S, C_3A, and C_4AF, on the other hand, disappear, reflecting an acceleration of hydration at this temperature, which is responsible for the increased mechanical properties of the mortars. Dehydration causes new C_2S and C_3S peaks to emerge, whereas CSH peaks decrease. The CSHs in question here would be those of 1st generation [50]. The amount of free lime increases with the addition of glass, while ettringite, monosulfate, and Stratlingite contents decrease due to water loss. All these transformations are attributed by Zhang et al. [56] to autoclave reactions. PVS and PVP addition show almost identical diffractograms for the different mixtures. At 600 °C, the Portlandite concentration of matrices with glass addition is higher than the control sample (OPC600) due to superior lime rehydration [87], but much lower at 25 °C due to general dehydration. Because of the increased dehydration of CSH and hydrated aluminates, the amounts of C_3A, C_2S, C_3S, and C_4AF rise with the addition of glass. Monosulfate and lime are abundant in OPC600, whereas CSH is more abundant in matrices with glass addition (PVS and PVP), implying that calcination accelerates the transformation of ettringite into monosulfate while having a lesser effect on CSH, mainly those produced secondarily. Monosulfate and free lime are the dominating minerals at 800 °C, primarily in OPC800, followed by CSH, which has not been entirely decomposed and is more relevant in matrices containing glass. C_2S and C_3S are more abundant at this stage, but the control sample appears to have allowed for higher disintegration of CSH; the other chemicals are

likewise more abundant, despite an overall decrease compared to lower temperatures. Amin et al. [96], show that the abundance of Portlandite is due to the recrystallization of the amorphous portion of Portlandite. In general, mortars containing PVS have a higher CSH content between 600 and 800 °C, resulting in higher mechanical strengths.

The spectra obtained by Hashem et al. [97], after the calcination of cement pastes with glass addition revealed an increase in CSH and Portlandite peaks for the control sample calcined at 300 °C, a decrease in Portlandite peaks for the sample with 20% glass addition, and the disappearance of the majority of peaks at 800 °C. Pan [98], discovered tiny ettringite peaks at room temperature that vanished after calcination at 500 °C, Portlandite, Belite, Alite, and Calcite peaks that reduced significantly between 500 and 800 °C, and Gehlenite and Akermanite peaks that were less sensitive to calcination. According to Rodier and Savastano [99], despite a 69% loss of mass after calcination for OPC due to dehydration of different phases of the cement paste, the inclusion of up to 20% glass reduces this loss of mass to 60%.

Overall, this work, like others in the literature, supports the assumption that the addition of glass improves the thermal durability of mortars, leading us to investigate heat migration in these matrices and deduce the energy properties of the materials developed; thus, the interest in studying the thermo-physical behavior of the various formulations.

3.2. Estimation of thermo-physical parameters

The asymmetrical hot plane approach was used to generate experimental thermograms, which were then used in a MATLAB program to calculate thermal effusivity, diffusivity, heat capacity, and conductivity. The results are shown by Fig. 14.

To assess the difference between the results of the various formulations, the relative variation of data to the control sample was calculated for each parameter, and the findings are displayed in Table 8.

These results suggest that the addition of PVS and PVP to OPC reduces the thermal conductivity of mortars. Indeed, it falls from 1.40 W/mK for OPC to 1.01 W/mK for PVS30 and 0.93 W/mK for PVP30, representing a −38.99% and −49.95% difference, respectively. As a result, the use of glass improves the thermal insulation of the cementitious matrix. Diffusivity increases by 10% when PVS and PVP are added to OPC, but declines significantly at 20% and 30% replacement, reaching −63.96% for PVS30 and -76.09% for PVP30. Glass, therefore, influences the structure of the matrix, limiting conductive heat transfer within it. Heat capacity, which is inversely proportional to diffusivity, decreases at 10% substitution by PVP (−21.09%) and PVS (−20.07%), before increasing at 20% and 30% substitution. With the addition of glass, thermal effusivity generally falls, most notably for PVS10 (−16.06%) and PVP10

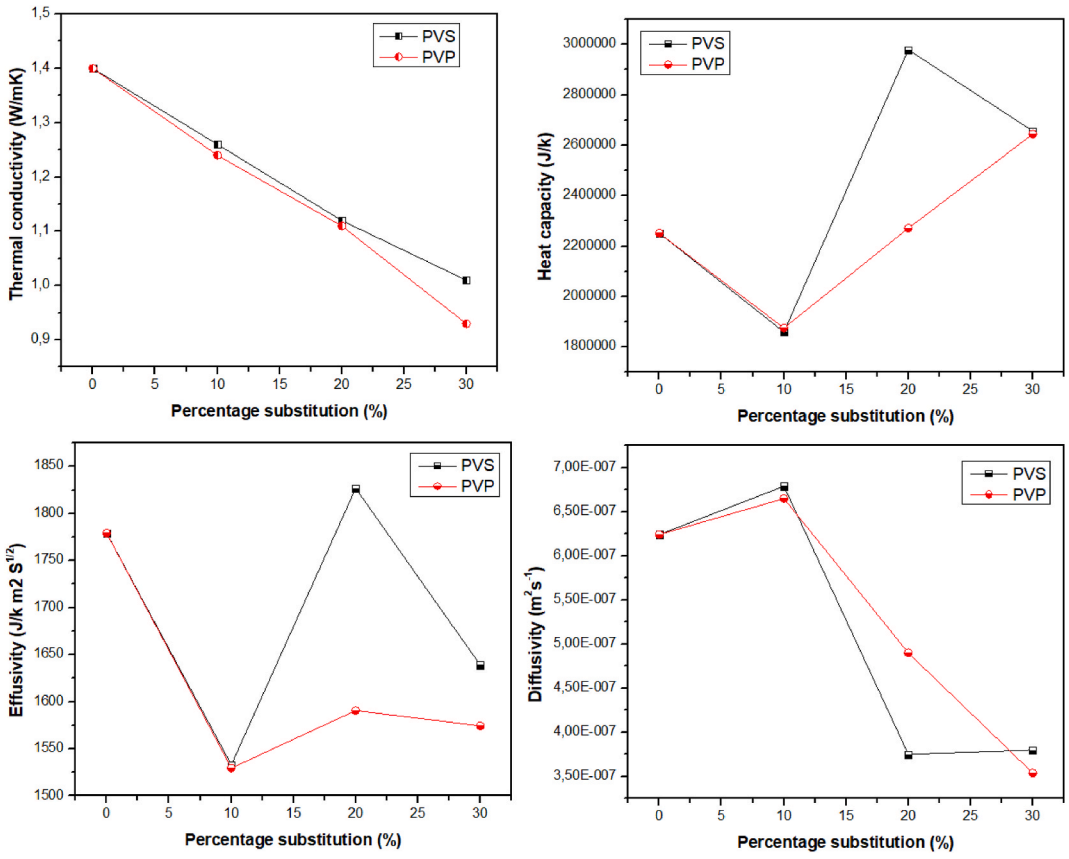

Fig. 14. Thermophysical properties of cement mortars with PVP and PVS addition.

Table 8
Thermo-physical properties of mortars with PVS and PVP addition.

Substitution content (%)	Thermophysical properties							
	Conductivity (W/mK)	Relative variation (%)	Diffusivity (m^2s^{-1})	Relative variation (%)	Heat capacity (J/k)	Relative variation (%)	Effusivity (J/k m^2 $s^{1/2}$)	Relative variation (%)
OPC	1.40	0.00	6.24^{E}-07	0.00	2252021.26	0.00	1779.15	0.00
PVS10	1.26	−11.24	6.79^{E}-07	8.14	1859759.44	−21.09	1532.93	−16.06
PVS20	1.12	−25.48	3.75^{E}-07	−66.00	2979400.02	24.41	1826.88	2.61
PVS30	1.01	−38.99	3.80^{E}-07	−63.96	2656504.90	15.23	1639.02	−8.55
PVP10	1.24	−12.67	6.65^{E}-07	6.17	1875553.29	−20.07	1529.64	−16.31
PVP20	1.11	−26.20	4.90^{E}-07	−27.31	2271834.14	0.87	1590.69	−11.85
PVP30	0.93	−49.95	3.54^{E}-07	−76.09	2644598.35	14.84	1574.4	−13.00

(−16.31%). As a result, the inclusion of glass powder improves the surface refractory properties.

The porosity of the matrices has a considerable influence on their thermo-physical properties; the more porous a material, the less heat it is expected to conduct [100]. In this regard, the study on ceramic materials shows that at pore volumes $V_P < 15\%$, as in the blends developed, the pores are generally closed and distributed throughout the material [101]. In this scenario, grain size has a greater influence on thermal conductivity than porosity. When V_p exceeds 15%, pores become linked (open porosity), blocking heat transfer in the material more effectively. Glass is also an amorphous material with low heat conductivity, as suggested by several studies [102,103]. This conductivity is lower than that of cement, according to Al-Zubaidi and Al-Tabbakh [104]. As stated by Abdel-Gawwad et al. [105], lead glass powder slurries are utilized to create materials with extremely low thermal conductivity. The combination of these reasons explains the observed decrease in thermal conductivity as well as PVP's addition of higher efficiency than PVS. Nasry et al. [38], notice the same conclusion after testing mortar formulations with up to 60% glass addition. Delgado et al. [106], contend that the presence of water in the cementitious matrix increases pores as well as conductivity. Despite having a higher E/C ratio in matrices with glass addition, drying the samples in the oven before testing allowed excess water, with a conductivity of around 0.59 W/mK, to be replaced by air with a conductivity of 0.03 W/mK, contributing to the lower conductivity of these matrices. Other factors influence the thermal behavior of materials as well. Dujardin et al. [107], demonstrated that pressure has a significant impact on thermal conductivity. Indeed, conductivity rises as pressure rises.

Babé et al. [40], reveal that the method of direct measurement of thermal conductivity is close to estimation by asymmetrical hot planes with a maximum standard variation of 9.3% on Sorghum bicolor fibers in adobes using the same way as in the current work. As a result, this approach can forecast thermal reinforcement with high accuracy. The literature review carried out on the properties of cementitious matrices amended with glass powder showed that despite the scarcity of work on the thermal behavior of these matrices, they are important and deserve more attention, since in general, the addition of glass has the effect of improving the thermal comfort of these matrices [43]. In this generally advantageous environment for the use of glass powder as a cementitious addition, it is appropriate to study the usefulness of modern prediction methods in lowering the cost of describing the materials produced. In this regard, the usual Artificial Neural Network (ANN) Multilayer Perceptron (MLP) approach could be utilized to forecast the mechanical behavior of mortar specimens based on physical parameters.

3.3. Artificial neural network prediction of compressive strength and flexural strength of mortars

The optimum parameters used to train the deep learning algorithms required to predict the flexural strength (RF-PVP, RF-PVS) and compressive strength (RC-PVP, RC-PVS) of mortars with PVP and PVS addition are shown in Table 9.

They state that "adam" was chosen as the optimization function for all models, while "relu" was chosen as the activation function for RC-PVP and RF-PVS, "tanh" for RF-PVP, and "sigmoid" for RC-PVP. The number of hidden neural layers is fixed in the PVP addition scenario (2 layers), but fluctuates in the RF addition case (1 and 4 layers) due to data unpredictability. This affects learning speed, which slows as the number of concealed layers grows. To learn RF-PVP (169), more neurons per layer are necessary, followed by RC-PVS (158), RF-PVS (88), and lastly (RC-PVP). In terms of batch size, RC-PVS (256) has the largest, followed by RC-PVP (32), RF-PVP (16), and RF-PVS (8). Based on these parameters, the algorithm's loss per epoch for each training is shown in Fig. 15.

Prediction suffers more losses during algorithm execution than flexural strength prediction. Indeed, RC-PVP and RC-PVS are more distant from zero (0) before the first 40 cycles than RF-PVP and RF-PVS. This means that the prediction efficiency of the Artificial Neural Network MLP approach for flexural strength prediction is higher than for compressive strength prediction. The dataset produced from laboratory measurements was separated into two groups: model training data (82.14% of the dataset) and data used to test the proposed models (17.86% of the dataset). Cross-validation was used to validate the models [108]. Fig. 16 depicts the graphs obtained from each model constructed using validation data.

The first graphical authentication model shows the validation of prediction models through the correlation curve of real-predicted data, with the predicted data crossed with the real data, converging variably towards the model that appears suitably representative of them. Fig. 17 shows a second type of validation using the error histogram (real values - projected values).

These histograms show that the errors have a normal distribution and a symmetrical structure around zero (0), which is typical of models with good prediction ability [54,109]. As a result, the learning models' performance might be considered pretty high. The models were then tested using the remaining data. Fig. 18 depicts cross-representations of real and predicted resistances.

Table 9
Optimal parameters of MLP learning algorithms used for prediction.

	Models			
Parameters	RC-PVP	RF-PVP	RC-PVS	RF-PVS
Learning rate	0.06	0.08	0.02	0.005
Number of hidden layers	2	2	1	4
Neurons per layer	64	169	158	88
Batch size	32	16	256	8
Activation function	relu	tanh	sigmoid	relu
Optimizer	adam	adam	adam	adam

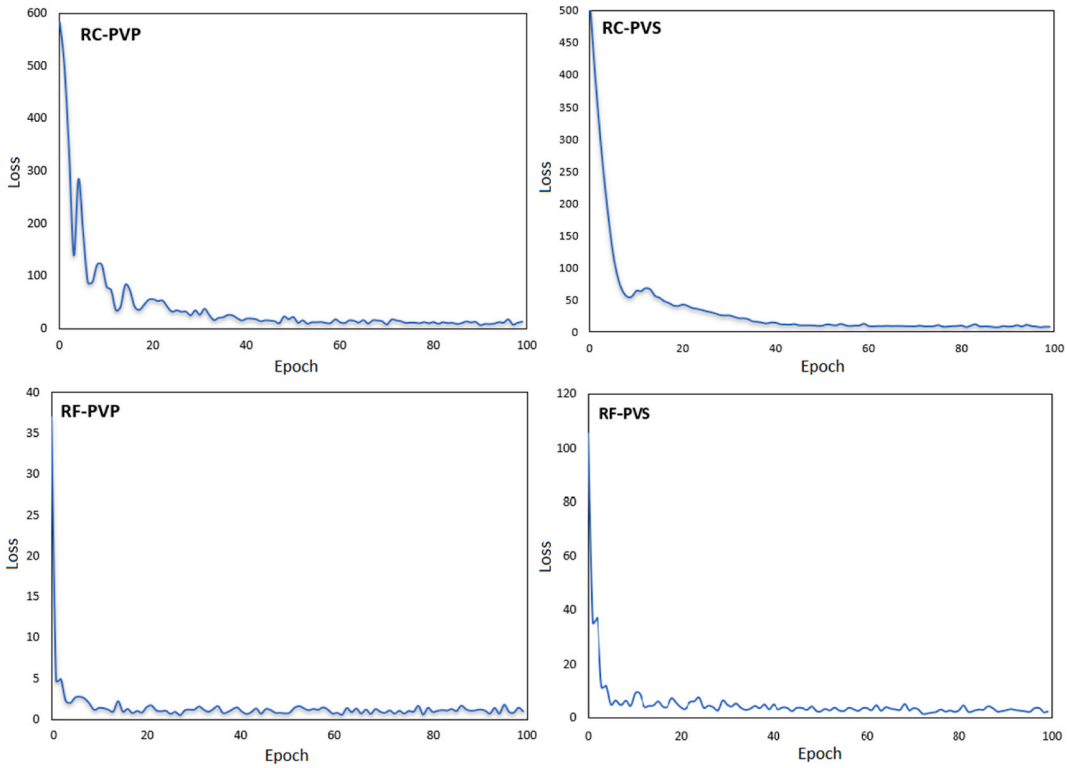

Fig. 15. Loss per epoch of each mechanical strength prediction algorithm.

Once again, the models come very close to reality for each prediction. To assess the effectiveness of the prediction method used, the statistical validation coefficients commonly considered are the correlation coefficient (R), mean absolute error (MAE), and root mean square error (RMSE) [110,111]. The values obtained for the models developed are recorded in Table 10.

The correlation coefficients between predicted and measured values for model training are $R^2 = 0.90$, $R^2 = 0.92$, $R^2 = 0.86$, and $R^2 = 0.91$, respectively for the RC-PVP, RF-PVP, RC-PVS, and RF-PVS models. The MAE and RMSE values are at most equal to 2.12 and 2.67 respectively; they are therefore relatively close to zero (0) and testify to a good degree of model certainty. The statistical coefficients of entrainment, therefore, express, with a high degree of certainty, the mechanical behavior of the specimens corresponding to the data used. Furthermore, the level of model certainty at validation also shows correlation coefficients $R^2 = 0.90$, $R^2 = 0.88$, $R^2 = 0.83$, and $R^2 = 0.77$, respectively for the RC-PVP, RF-PVP, RC-PVS, and RF-PVS models. These results, all close to 1, confirm the effectiveness of the MLP method in predicting the mechanical strengths of mortars with glass addition.

Deep learning methods, notably ANN's Multilayer Perceptron Method, have proven their worth in forecasting the mechanical strengths of cementitious matrices. The work of Abellán-Garca et al. [58] in particular, showed that MLP was effective in forecasting the strengths of ultra-high-performance concretes, with correlation values ranging from $R^2 = 0.96$ to $R^2 = 0.988$ for RMSEs not exceeding 2.638 MPa. Zhang et al. [112] predicted the mechanical strengths of concretes with additional silica fume and fly ash with R^2 values in the order of 0.9986. MLPs were used to estimate the strengths of mortars using rice husks and recycled asphalt paving stones, with R^2 values reaching 0.9902 [113].

Other studies [114], predicted the mechanical strengths of concretes containing recycled aggregates using linear regression applied in ANN, with $R^2 = 0.9607$ and $R^2 = 0.9855$, respectively. Qadir et al. [54], demonstrated the efficiency of the Vipulanandan

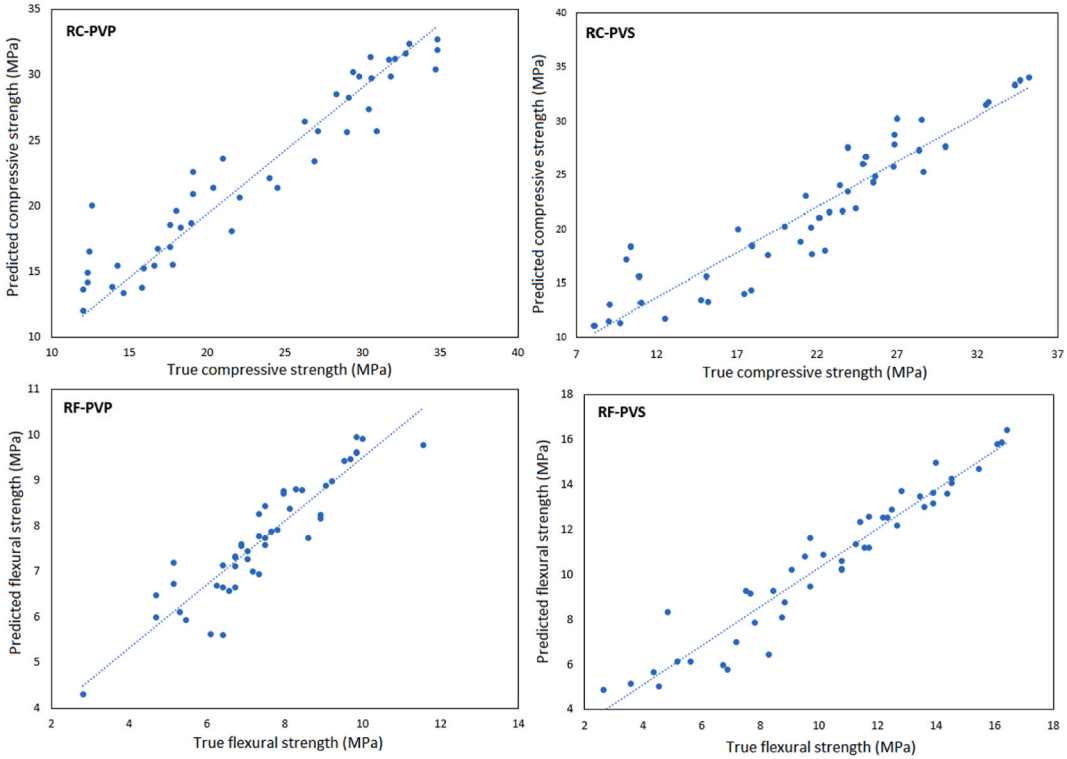

Fig. 16. Cross-validation for model training.

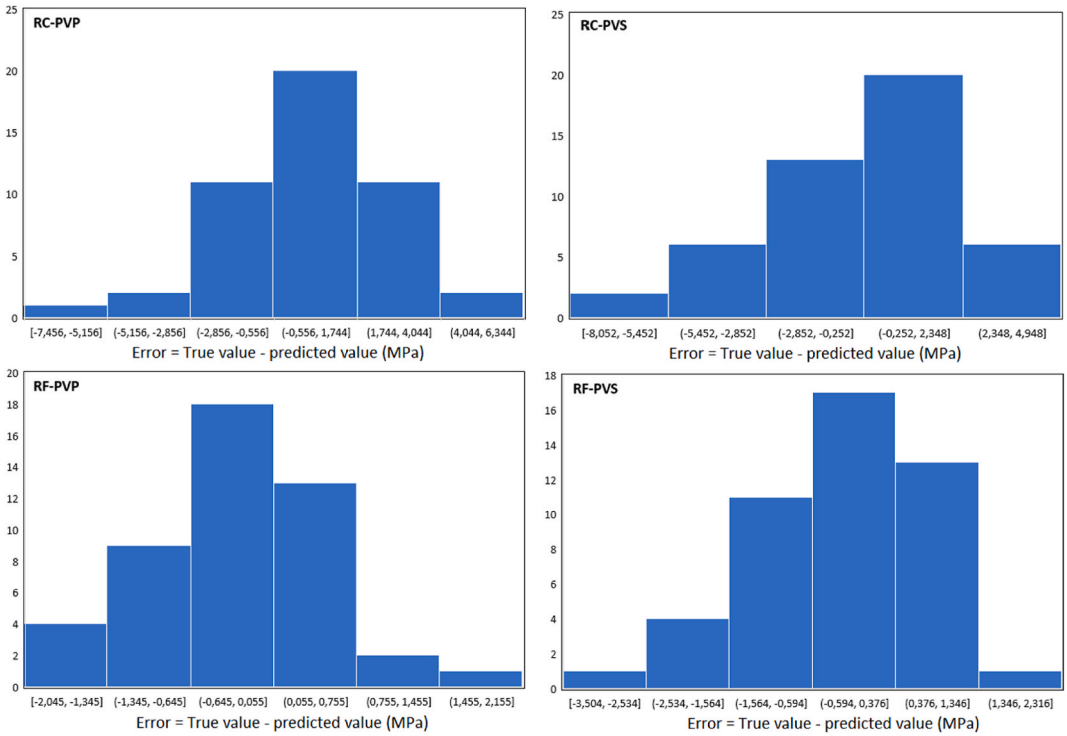

Fig. 17. Error histogram validation.

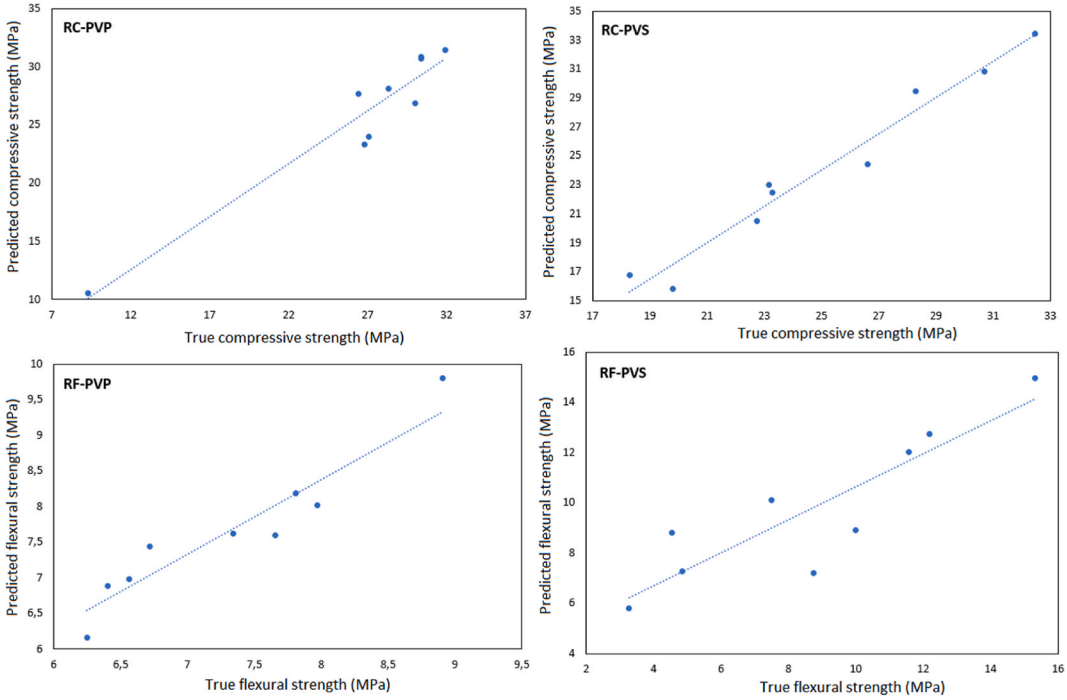

Fig. 18. Cross-validation for model testing.

Table 10
Statistical coefficients for validating mechanical strength prediction models.

MODEL	TYPE	R^2	MAE	RMSE
RC-PVP	Train	0.90	1.78	2.32
	Test	0.90	1.52	1.98
RF-PVP	Train	0.92	0.58	0.76
	Test	0.88	0.37	0.46
RC-PVS	Train	0.86	2.12	2.67
	Test	0.83	1.47	1.86
RF-PVS	Train	0.91	0.78	1.02
	Test	0.77	1.75	2.14

correlation model and the Hoek-Brown model in predicting the strengths of mortars with fly ash added, with R^2 values ranging from 0.80 to 0.98 and RMSE values ranging from 0.057 to 6.4. The slew of works and prediction methods presented by some authors [113–117], illustrate their importance in the study of materials and make available a range of options likely to support the perpetuity of research always in search of optimization.

4. Conclusion

Investigations into the acid and calcination durability, thermal and thermo-physical properties, and prediction of mechanical strengths of mortars incorporating soda-lime glass on one hand and lead glass on the other revealed that:

- The acid attack was mitigated by the addition of PVP and PVS. At an early age (2 days), mortars with 20% PVP and PVS additions demonstrated the best acid resistance, while mortars with 10% additions demonstrated greater acid resistance at an older age (28 days). Sulfuric acid damaged mortars more aggressively than hydrochloric acid;
- The thermal study revealed that the stepwise inclusion of glass reduced mass loss owing to calcination. PVP addition resulted in fewer losses than PVP addition. The percentages decreased from 22% for OPC to −19.5% for PVS30 and -18% for PVP30. Flexural strengths in calcined mortars declined from −20.1% at 400 °C (PVS10400) to −93.3% at 800 °C (PVS20800), whereas compressive values were higher at 400 °C than at ambient temperature (up to 48.6% for PVP20400). At 600 °C, a 20% glass additive kept the mortar fire-resistant (18.5% for PVP20600 and 23.8% for PVS20600). All formulations mechanically deteriorated at 800 °C (up to −61.9% for PVP30800). Mortars with 20% glass addition had the best mechanical performance. The hydrated product, interacted in autoclave reactions between 400 and 600 °C to improve mechanical properties, whereas extensive dehydration of the matrices

resulted in significant reductions in strength at 800 °C. Because of its increased pozzolanic activity, soda-lime glass powder showed better mechanical behavior than lead glass powder;

- The addition of glass reduced thermal conductivity proportionally to its concentration. PVS30 was reduced by −38.99%, whereas PVP30 was reduced by −49.95%. Diffusivity increased just slightly at 10% addition (8.14 for PVS10 and 6.17 for PVP10) before dropping considerably at 20% and 30% addition, reaching −66% (PVS20) and −76.09 for PVP30, respectively. Heat capacity fell after a 10% addition and then increased between 20 and 30%. Effusivity decreased up to 30% with the addition of PVP and PVS, with a maximum of 16.31% (PVP10). Based on these findings, it was evident that glass powder improved the thermal insulation of cementitious matrices and thus their thermal comfort;
- When trained on the database, the models developed to predict mechanical strengths using MLP produced correlation coefficients of $R^2 = 0.90$, $R^2 = 0.92$, $R^2 = 0.86$, and $R^2 = 0.91$ for the RC-PVP, RF-PVP, RC-PVS, and RF-PVS models, respectively. At validation, these coefficients were $R^2 = 0.90$, $R^2 = 0.88$, $R^2 = 0.83$, and $R^2 = 0.77$ for RC-PVP, RF-PVP, RC-PVS, and RF-PVS, respectively. MAE levels in both cases reached a maximum of 2.12, while RMSE values reached a maximum of 2.67.

The following future work is planned within the framework of this study: the search for the best numerical method for predicting each property of the produced matrices; the life cycle analysis of each type of glass used as supplementary cementitius material; the optimization of mortar and concrete qualities by investigating ternary cements with glass addition.

Funding

The authors received no financial support for the research, authorship, and/or publication of this article.

Data availability

All data generated or analyzed during this study are included in this article.

Compliance with ethical standards

This manuscript has not been published elsewhere in any form or language and has not been submitted to more than one journal for simultaneous consideration.

CRediT authorship contribution statement

Yannick Tchedele Langollo: Writing – review & editing, Writing – original draft, Visualization, Validation, Software, Resources, Methodology, Investigation, Funding acquisition, Formal analysis, Data curation, Conceptualization. **Essomba Essomba Juste Constant:** Writing – review & editing, Writing – original draft, Resources, Methodology, Funding acquisition, Formal analysis, Data curation. **Emini Pierre Boris Gael:** Writing – review & editing, Writing – original draft, Software, Resources, Methodology, Formal analysis, Conceptualization. **Boroh Andre William:** Writing – review & editing, Writing – original draft, Validation, Software, Funding acquisition, Conceptualization. **Mambou Ngueyep Luc Leroy:** Writing – review & editing, Writing – original draft, Validation, Supervision, Methodology. **Tchamba Arlin Bruno:** Writing – review & editing, Writing – original draft, Validation, Supervision, Resources, Methodology, Conceptualization. **Ngounouno Ismaïla:** Writing – review & editing, Writing – original draft, Visualization, Supervision, Methodology, Funding acquisition, Conceptualization.

Declaration of competing interest

The authors declare that they have no known competing financial interests or personal relationships that could have appeared to influence the work reported in this paper.

Acknowledgements

The Authors are grateful to Professor Nathalie Fagel (AGES Lab), University of Liege, Belgium, for her assistance in conducting some analyses in her Institution. We dedicate this effort to the memory of our colleague Bodang Mikael Moudoh, with whom we had fruitful collaboration throughout our research journey.

References

[1] C.R. Gagg, Cement and concrete as an engineering material: an historic appraisal and case study analysis, Eng. Fail. Anal. 40 (2014) 114–140.
[2] H. Van Damme, Concrete material science: past, present, and future innovations, Cement Concr. Res. 112 (2018) 5–24.
[3] G. Habert, Assessing the environmental impact of conventional and 'green'cement production, in: Eco-efficient Construction and Building Materials, 2014, pp. 199–238, https://doi.org/10.1533/9780857097729.2.199.
[4] UN Environment and International Energy Agency, Global Status Report 2017: towards a Zero-Emission, Efficient, and Resilient Buildings and Construction Sector, UNEnvironment, Paris, 2017. http://www.worldgbc.org/sites/default/files/UNEP%20188_GABC_en%20%28web%29. pdf. (Accessed 25 April 2018).

[5] R. Rajaramakrishna, J. Kaewkhao, Glass material and their advanced applications, KnE Soc. Sci. 2019 (2019) 796–807, https://doi.org/10.18502/kss.v3i18.4769.
[6] D.E. Koranyi, Surface Properties of Silicate Glass, Akadémiai Kiadó, Budapest, 1963.
[7] M. Saito, M. Shukuya, Energy and material use in the production of insulating glass windows, Sol. Energy 58 (4–6) (1996) 247–252.
[8] A. Schmitz, J. Kaminski, B.M. Scalet, A. Soria, Energy consumption and CO2 emissions of the European glass industry, Energy Pol. 39 (1) (2011) 142–155, https://doi.org/10.1016/j.enpol.2010.09.022.
[9] C.D. Westbroek, J. Bitting, M. Craglia, J.M. Azevedo, J.M. Cullen, Global material flow analysis of glass: from raw materials to end of life, J. Ind. Ecol. 25 (2) (2021) 333–343.
[10] J. Harder, Glass Recycling – Current Market Trends, 2018. https://www.recovery-worldwide.com/en/artikel/glass-recycling-current-market-trends_3248774.html.
[11] H. Nguyen, Valorisation du verre dans le béton Etude expérimentale du comportement de pâte de ciment et du mortier : rhéologie, mécanique et durabilité. *Thèse de doctorat en cotutelle*, vol. 119, Université d'Aix-Marseille, Institut de mécanique du Viet Nam, 2013. http://www.theses.fr/2013AIXM4793/document.
[12] M. Kaya, The effect of micro-SiO2 and micro-Al2O3 additive on the strength properties of ceramic powder-based geopolymer pastes, J. Mater. Cycles Waste Manag. 24 (1) (2022) 333–350.
[13] J. Lehne, F. et Preston, Making Concrete Change: Innovation in Low-carbon Cement and Concrete, 2018. Chatham House Report, ISBN:9781784132729.
[14] I. Rachida, Mécanismes d'action des fines et des granulats de verre sur la réaction alcali-silice et la réaction pouzzolanique, Thèse de doctorat de l'université de Toulouse, Toulouse, 2009.
[15] C. Shin, K. Zheng, A review on the use of waste glasses in the production of cement and concrete, Resour. Conserv. Recycl. 52 (2007) 234–247.
[16] C.H. Chen, R. Huang, J.K. Wu, C.C. Yang, Waste E-glass particles used in cementitious mixtures, Cement Concr. Res. 36 (3) (2006) 449–456.
[17] L.L. Duna, N.G.A. Nguimeya, A.B. Tchamba, N. Billong, E. Kamseu, E. Qoku, T.S. Alomayri, T.A. Bier, Engineering and mineralogical properties of Portland cement used for building and road construction in Cameroon, Int. J. Pav. Res. Technol. 15 (4) (2021) 821–834.
[18] K.L.V.E. Samen, R.N. Yanou, C.K.M. Fonzeu, L.A.R. Kamgue, A.B. Tchamba, G.G.M. Tchapga, L. Yang, B. Mempouo, Engineering properties of soda-lime glass powder on Portland cement CEM IV-B-L mortar, J. Build. Pathol. Rehab. 7 (27) (2022) 15, https://doi.org/10.1007/s41024-022-00164-3.
[19] K. Yamada, S. Ishiyama, Maximum dosage of glass cullet as fine aggregate in mortar, in: Achieving Sustainability in Construction: Proceedings of the International Conference Held at the University of Dundee, Thomas Telford Publishing, Scotland, UK, 2005, pp. 185–192.
[20] M. Mirzahosseini, K.A. Riding, Influence of different particle sizes on reactivity of finely ground glass as supplementary cementitious material (SCM), Cement Concr. Compos. (2014) 95–105.
[21] V. Shevchenko, G. Kotsay, Determination of glass waste allowable amount used as an additive to Portland cement, J. Civil Eng. Environ. Arch. (2015) 403–410.
[22] N. Tamanna, M.S. Norsuzailina, R. Tuladhar, T.C.L. Delsye, I. Yakub, Pozzolanic properties of glass powder in cement paste, J. Eng. Sci. Technol. 7 (2) (2016) 75–81.
[23] G. Vijayakumar, H. Vishaliny, D. Govindarajulu, Studies on glass powder as partial replacement of cement in concrete production, Int. J. Emerg. Technol. Adv. Eng. 3 (2) (2013) 153–157. February.
[24] A. Abdullah, The influence of waste glass powder as a pozzolanic material in concrete, Int. J. Civ. Eng. Technol. 7 (6) (2016) 131–148.
[25] I. Ansari, S. Sheetal, Utilization of glass powder as a partial replacement of cement and its effect on concrete strength – a review, Int. J. Adv. Mech. Civil Eng. 3 (1) (2016) 75–79.
[26] A. Rahma, E.N. Nabil, I.I. Sherzad, Effect of glass powder on the compression strength and the workability of concrete, Civ. Environ. Eng. (2017) 1–10.
[27] H. Elaqra, R. Rustom, Effect of using glass powder as cement replacement on rheological and mechanical properties of cement paste, Construct. Build. Mater. 179 (2018) 326–335.
[28] I.O. Yasser, Hesham A. Yahia, O.S. Manal, M. Talal, Effects of wood ash and waste glass powder on properties of concrete in terms of workability and compressive strength in jaresh city, Open J. Civ. Eng. (2017) 423–431.
[29] G. Liu, M.V.A. Florea, H.J.H. Brouwers, Performance evaluation of sustainable high strength mortars incorporating high volume waste glass as binder, Construct. Build. Mater. 202 (2019) 574–598.
[30] K. Sobolev, P. Turker, S. Soboleva, G. Iscioglu, Utilization of waste glass in ECO-cement: strength properties and microstructural observations, Waste Manag. 27 (2007) 971–976.
[31] N. Schwarz, N. et Neithalath, Influence of a fine glass powder on cement hydration: comparison to fly ash and modeling the degree of hydration, Cement Concr. Res. 38 (4) (2008) 429–436.
[32] S. Correia, F. Souza, G. Dienstmann, A.M. Segadaes, Assessment of the recycling potential of fresh concrete waste using a factorial design of experiments, Waste Manag. 29 (2009) 2886–2891.
[33] A. Younsi, Carbonatation de bétons à forts taux de substitution du ciment par des additions minérales, Université de La Rochelle, 2011. Doctoral dissertation.
[34] D. Wan, W. Zhang, Y. Tao, Z. Wan, F. Wang, S. Hu, Y. He, The impact of Fe dosage on the ettringite formation during high ferrite cement hydration, J. Am. Ceram. Soc. 104 (7) (2021) 3652–3664.
[35] K. Sobolev, M. Kozhukhova, K. Sideris, E. Menéndez, M. Santhanam, Alternative supplementary cementitious materials, in: Properties of Fresh and Hardened Concrete Containing Supplementary Cementitious Materials, Springer, Cham, 2018, pp. 233–282.
[36] R.O.A. Rahman, M.I. Ojovan, Sustainability of cementitious structures, systems, and components (SSC's): long-term environmental stressors, in: Sustainability of Life Cycle Management for Nuclear Cementation-Based Technologie, Woodhead Publishing, 2021, pp. 181–232.
[37] M.N.N. Khan, J.C. Kuri, P.K. Sarker, Sustainable use of waste glass in alkali activated materials against H2SO4 and HCl acid attacks, Cleaner Eng. Technol. 6 (2022) 100354.
[38] O. Nasry, A. Samaouali, S. Belarouf, A. Moufakkir, H. Sghiouri El Idrissi, H. Soulami, Y. Younes El-Rhaffari, M. Hraita, F.S. Ed-Dîn, A. Hafidi-Alaoui, Thermophysical properties of cement mortar containing waste glass powder, Crystals 11 (5) (2021) 488.
[39] M.M. Radwan, S.M. Nagi, Hydration behavior and formation of strätlingite compound (C2ASH8) in a bio-cement based on tri-calcium silicate and mono-calcium aluminate for dental applications: influence of curing medium, Bull. Natl. Res. Cent. 46 (1) (2022) 1–14.
[40] C. Babé, D.K. Kidmo, A. Tom, R.R.N. Mvondo, R.B.E. Boum, N. Djongyang, Thermomechanical characterization and durability of adobes reinforced with millet waste fibers (sorghum bicolor), Case Stud. Constr. Mater. 13 (2020) e00422.
[41] E.K. Kowa, J.C. Damfeu, U.J. Pettang, J. Ducourneau, P. Woafo, C. Pettang, Thermophysical and mechanical characterization of poto-poto compressed blocks for use as fill material, Mater. Sci. Appl. 12 (10) (2021) 437–459.
[42] T.E. Mbou, P.W. Huisken Mejouyo, P.A. Ndema Ewane, C. Damfeu, P. Meukam, E. Njeugna, Effect of particle sizes on physical, thermal and mechanical behavior of a hybrid composite with polymer matrix with raffia vinifera cork and Bambusa vulgaris, Polym. Bull. (2023) 1–21.
[43] J.M. Santiago, F. de Souza Clementino, I.G.C. da Conceição, H.F. de Sousa, H.C. dos Santos, Effects on the properties of cementitious composites using waste glass powder (WGP) as a partial replacement for cement, Int. J. Innov. Educ. Res. (1) (2022) 307–324.
[44] O. Gencel, O.Y. Bayraktar, G. Kaplan, O. Arslan, M. Nodehi, A. Benli, A. Gholampour, T. Ozbakkaloglu, Lightweight foam concrete containing expanded perlite and glass sand: physico-mechanical, durability, and insulation properties, Construct. Build. Mater. 320 (2022) 126187.
[45] F. Koksal, T. Nazlı, A. Benli, O. Gencel, G. Kaplan, The effects of cement type and expanded vermiculite powder on the thermo-mechanical characteristics and durability of lightweight mortars at high temperature and RSM modelling, Case Stud. Constr. Mater. 15 (2021) e00709.
[46] G. Kaplan, U. Coskan, A. Benli, O.Y. Bayraktar, A.B. Kucukbaltacı, The impact of natural and calcined zeolites on the mechanical and durability characteristics of glass fiber reinforced cement composites, Construct. Build. Mater. 311 (2021) 125336.
[47] O.Y. Bayraktar, G. Kaplan, O. Gencel, A. Benli, M. Sutcu, Physico-mechanical, durability and thermal properties of basalt fiber reinforced foamed concrete containing waste marble powder and slag, Construct. Build. Mater. 288 (2021) 123128.
[48] V. Zivica, A. Bajza, Acidic attack of cement-based materials—a review: Part 1. Principle of acidic attack, Construct. Build. Mater. 15 (8) (2001) 331–340.
[49] S. Chatterji, Mechanism of the CaCl2 attack on Portland cement concrete, Cement Concr. Res. 8 (4) (1978) 461–467.

[50] R.K. Ibrahim, R. Hamid, M.R. Taha, Fire resistance of high-volume fly ash mortars with nanosilica addition, Construct. Build. Mater. 36 (2012) 779–786.
[51] F. Koksal, E.T. Kocabeyoglu, O. Gencel, A. Benli, The effects of high temperature and cooling regimes on the mechanical and durability properties of basalt fiber reinforced mortars with silica fume, Cement Concr. Compos. 121 (2021) 104107.
[52] H. Eskandaria, M.G. Nikb, M.M. Eidia, Prediction of mortar compressive strengths for different cement grades in the vicinity of sodium chloride using ANN, Procedia Eng. 150 (2016) 2185–2192.
[53] M. Apostolopoulou, D.J. Armaghani, A. Bakolas, M.G. Douvika, A. Moropoulou, P.G. Asteris, Compressive strength of natural hydraulic lime mortars using soft computing techniques, Procedia Struct. Integr. (2019) 914–923.
[54] W. Qadir, K. Ghafor, M. Ahmed, Characterizing and modeling the mechanical properties of the cement mortar modified with fly ash for various water-to-cement ratios and curing times, Adv. Civ. Eng. (2019) 1–11.
[55] M. Kaya, Z.B. Yıldırım, F. Köksal, A. Beycioğlu, I. Kasprzyk, Evaluation and multi-objective optimization of lightweight mortars parameters at elevated temperature via Box–Behnken optimization approach, Materials 14 (23) (2021) 7405.
[56] J. Zhang, Y. Zhao, H. Li, Experimental investigation and prediction of compressive strength of ultra-high performance concrete containing supplementary cementitious materials, Adv. Mater. Sci. Eng. 2017 (2017).
[57] M.A. Getahun, S.M. Shitote, Z.C.A. Gariy, Artificial neural network based modelling approach for strength prediction of concrete incorporating agricultural and construction wastes, Construct. Build. Mater. 190 (2018) 517–525.
[58] J. Abellán-García, J.G. Fernandez, T.N. Castellanos, Properties prediction of environmentally friendly ultra-high-performance concrete using artificial neural networks, Eur. J. Environ. Civil Eng. 26 (6) (2020) 2319–2343.
[59] O.Y. Bayraktar, S.S.T. Eshtewı, A. Benli, G. Kaplan, K. Toklu, F. Gunek, The impact of RCA and fly ash on the mechanical and durability properties of polypropylene fibre-reinforced concrete exposed to freeze-thaw cycles and MgSO4 with ANN modeling, Construct. Build. Mater. 313 (2021) 125508.
[60] NF EN 197-1, Ciment - Partie 1 : composition, spécifications et critères de conformité des ciments courants, AFNOR, 2012.
[61] NF EN 197-1, Ciment - Partie 1 : composition, spécifications et critères de conformité des ciments courants, AFNOR, 2012.
[62] ASTM E119-19, Standard Test Methods for Fire Tests of Building Construction and Materials, ASTM International, West 433Conshohocken, USA, 2000.
[63] ASTM C267, Standard Test Methods for Chemical Resistance of Mortars, Grouts, and Monolithic Surfacings and Polymer Concretes, ASTM International, West 433Conshohocken, USA, 2020.
[64] H. Yu, B.M. Wilamowski, Levenberg–marquardt training, in: Intelligent Systems, CRC Press, 2018, pp. 1–12.
[65] Y. LeCun, Y. Bengio, G. Hinton, Deep learning, Nature 521 (7553) (2015) 436–444.
[66] K. Ramasubramanian, A. Singh, Deep learning using keras and TensorFlow, in: Machine Learning Using R, Apress, Berkeley, CA, 2019, pp. 667–688, https://doi.org/10.1007/978-1-4842-4215-5_11.
[67] H. Siad, H.A. Mesbah, S. Kamali Bernard, H. Khelafi, M. Mouli, Influence of natural pozzolan on the behavior of self-compacting concrete under sulphuric and hydrochloric acid attacks, comparative study, Arabian J. Sci. Eng. (2010) 183–195.
[68] P. Dinakar, K.G. Babu, M. Santhanam, Durability properties of high-volume fly ash self compacting concretes, Cement Concr. Compos. 30 (2008) 880–886.
[69] N.T. Fattuhi, B.P. Hughes, The performance of cement paste and concrete subjected to sulphuric acid attack, Cement Concr. Res. 18 (1988) 545–553.
[70] K. Torri, M. Kawamura, Effects of fly ash and silica fume on the resistance of mortar to sulphuric acid and sulphate attack, Cement Concr. Res. 24 (2) (1994) 361–570.
[71] H. Siad, M. Lachemi, M. Sahmaran, K.M.A. Hossain, Effect of glass powder on sulfuric acid resistance of cementitious materials, Construct. Build. Mater. 113 (2016) 163–173.
[72] H.Y. Wang, The effect of the proportion of thin film transistor–liquid crystal display (TFT–LCD) optical waste glass as a partial substitute for cement in cement mortar, Construct. Build. Mater. (25) (2011) 791–797.
[73] L. Bertolini, M. Carsana, M. Frassoni, M. Gelli, Pozzolanic additions for durability of concrete structures, Proc. Inst. Civil Eng.-Constr. Mater. 164 (6) (2011) 283–291.
[74] M.T. Bassuoni, M. Nehdi, M. Amin, Self-Compacting concrete: using limestone to resist sulfuric acid, Constr. Mater. 160 (2007) 113–123.
[75] C. Hall, P. Barnes, A.D. Billimore, A.C. Jupe, X. Turrillas, Thermal decomposition of ettringite Ca6[Al(OH)6]2(SO4)3·26H2O, J. Chem. Soc., Faraday Trans. 92 (12) (1996) 2125–2129.
[76] Q. Zhou, F. Glasser, Thermal stability and decomposition mechanisms of ettringite at $< 120^{\circ}C$, Cement Concr. Res. 31 (2001) 1333–1339.
[77] E. Stepkowska, J. Blanes, F. Franco, C. Real, J. Pérez-Rodríguez, Phase transformation on heating of an aged cement paste, Thermochim. Acta 420 (1–2) (2004) 79–87.
[78] F. Paulik, J. Paulik, M. Arnold, Thermal decomposition of gypsum, Thermochim. Acta 200 (1992) 195–204.
[79] I.Y. Elbeyli, E.M. Derun, J. Gülen, S. Pişkin, Thermal analysis of borogypsum and its effects on the physical properties of Portland cement, Cement Concr. Res. 33 (11) (2003) 1729–1735.
[80] J.M. David, R.M. De Jesus, R.P. Mendoza Jr., Quantification of hydration products in rice husk ash (RHA)-blended cement concrete with crumb waste rubber tires (CWRT) & its correlation with mechanical performance, GEOMATE J. 23 (99) (2022) 126–133.
[81] P. Mounanga, A. Khelidj, A. Loukili, V. Baroghel-Bouny, Predicting Ca $(OH)_2$ content and chemical shrinkage of hydrating cement pastes using analytical approach, Cement Concr. Res. 34 (2) (2017) 255–265. Elsevier.
[82] M.U. Salim, M.A. Mosaberpanah, Mechanical and durability properties of high-performance mortar containing binary mixes of cenosphere and waste glass powder under different curing regimes, J. Mater. Res. Technol. 13 (2021) 602–617.
[83] H.E.H. Seleem, A.M. Rashad, T. Elsokary, Effect of elevated temperature on physico-mechanical properties of blended cement concrete, Construct. Build. Mater. 25 (2) (2011) 1009–1017.
[84] D. Vaičiukynienė, G. Skipkiūnas, M. Daukšys, V. Sasnauskas, Cement hydration with zeolite-based additive, Chemija 24 (4) (2013) 271–278.
[85] R.S. Lin, X.Y. Wang, H.S. Lee, H.K. Cho, Hydration and microstructure of cement pastes with calcined Hwangtoh clay, Materials 12 (3) (2019) 458.
[86] D. Govindarajan, R. Gopalakrishnan, Spectroscopic studies on Indian Portland cement hydrated with distilled water and sea water, Front. Sci. 1 (1) (2011) 21–27.
[87] M.A. Tantawy, Effect of high temperatures on the microstructure of cement paste, J. Mater. Sci. Chem. Eng. 5 (11) (2017) 33.
[88] H.A. Abdel-Gawwad, S.A. El-Enein, M. Heikal, S. Abd El-Aleem, A.A. Amer, I.M. El-Kattan, Synergistic effects of curing conditions and magnesium oxide addition on the physico-mechanical properties and firing resistivity of Portland cement mortar, Construct. Build. Mater. 176 (2018) 676–689.
[89] M.M. Alonso, M. Palacios, F. Puertas, Effect of polycarboxylate-ether admixtures on calcium aluminate cement pastes. Part 2: hydration studies, Ind. Eng. Chem. Res. (52) (2013) 17330, https://doi.org/10.1021/ie401616f.
[90] R. Ylmén, U. Jäglid, B.M. Steenari, I. Panas, Early hydration and setting of Portland cement monitored by IR, SEM and Vicat techniques, Cement Concr. Res. 39 (5) (2009) 433–439.
[91] F. Matossi, Vibration frequencies and binding forces in some silicate groups, J. Chem. Phys. (17) (1949) 679, https://doi.org/10.1063/1.1747369.
[92] J.P. Bombled, Rhéologie du béton frais, Publication Technique N°161, C.E.R.I.L.H., Paris, 1964.
[93] K.E. Peray, Cement Manufacturers Hand Book, Chemical Publishing Company Inc, New York, 1979.
[94] J. Newman, S.B. Choo, Advanced Concrete Technology, Constituent Materials, Elsevier, Burlington, 2003.
[95] F. Song, Z. Yu, F. Yang, Y.F. Liu, Y. Lu, Strätlingite and calcium hemicarboaluminate hydrate in belite-calcium sulphoaluminate cement, Ceramics 58 (2014) 269–274.
[96] M.S. Amin, S.M.A. El-Gamal, F.S. Hashem, Fire resistance and mechanical properties of carbon nanotubes–clay bricks wastes (Homra) composites cement, Construct. Build. Mater. 98 (2015) 237–249.
[97] F.S. Hashem, E.E. Hekal, M.A. Naby, F.A. Selim, Mechanical properties and durability performance against fire, gamma ray and bio-fouling of hardened Portland cement pastes incorporating lead bearing wastes, Mater. Chem. Phys. 272 (2021) 124997.
[98] Z. Pan, Z. Tao, T. Murphy, R. Wuhrer, High temperature performance of mortars containing fine glass powders, J. Clean. Prod. 162 (2017) 16–26.

[99] L. Rodier, H. Savastano Jr., Use of glass powder residue for the elaboration of eco-efficient cementitious materials, J. Clean. Prod. 184 (2018) 333–341.
[100] A. Stolarska, J. Strzałkowski, The thermal parameters of mortars based on different cement type and W/C ratios, Materials 13 (19) (2020) 4258.
[101] D.S. Smith, A. Alzina, J. Bourret, B. Nait-Ali, F. Pennec, N. Tessier-Doyen, K. Otsu, H. Matsubara, P. Elser, U.T. Gonzenbach, Thermal conductivity of porous materials, J. Mater. Res. 28 (17) (2013) 2260–2272.
[102] P. Sikora, E. Horszczaruk, K. Skoczylas, T. Rucinska, Thermal properties of cement mortars containing waste glass aggregate and nanosilica, Procedia Eng. 196 (2017) 159–166.
[103] K. Gorospe, E. Booya, H. Ghaednia, S. Das, Strength, durability, and thermal properties of glass aggregate mortars, J. Mater. Civ. Eng. 31 (10) (2019) 04019231.
[104] A.B. Al-Zubaidi, A.A. Al-Tabbakh, Recycling glass powder and its use as cement mortar applications, Int. J. Sci. Eng. Res. 7 (2016) 555–564.
[105] H.A. Abdel-Gawwad, M.S. Mohammed, M.A. Arif, H. Shoukry, Reuse of lead glass sludge in the fabrication of thermally insulating foamed glass with outstanding properties and high Pb-stabilization, Environ. Sci. Pollut. Control Ser. (2022) 1–16.
[106] J.M.P.Q. Delgado, A.S. Guimarães, V.P. De Freitas, I. Antepara, V. Kočí, R. Černý, Salt damage and rising damp treatment in building structures, Adv. Mater. Sci. Eng. (2016), https://doi.org/10.1155/2016/1280894.
[107] N. Dujardin, T. Salem, V. Feuillet, M. Fois, L. Ibos, C. Poilâne, R. Manuel, Measurement of pore size distribution of building materials by thermal method, Construct. Build. Mater. 245 (2020) 118417.
[108] A. Vabalas, E. Gowen, E. Poliakoff, A.J. Casson, Machine learning algorithm validation with a limited sample size, PLoS One 14 (11) (2019) e0224365.
[109] A.W. Boroh, S.K. Lawou, M.L. Mfenjou, I. Ngounouno, Comparison of geostatistical and machine learning models for predicting geochemical concentration of iron: case of the Nkout iron deposit (south Cameroon), J. Afr. Earth Sci. 195 (2022) 104662.
[110] H.R. Tavakoli, O.L. Omran, M.F. Shiade, S.S. Kutanaei, Prediction of combined effects of fibers and nanosilica on the mechanical properties of self-compacting concrete using artificial neural network, Lat. Am. J. Solid. Struct. 11 (2014) 1906–1923.
[111] J. Abellán-García, Four-layer perceptron approach for strength prediction of UHPC, Construct. Build. Mater. 256 (2020) 119465.
[112] J. Zhang, M. Sun, D. Hou, Z. Li, External sulfate attack to reinforced concrete under drying-wetting cycles and loading condition: numerical simulation and experimental validation by ultrasonic array method, Construct. Build. Mater. 139 (2017) 365–373.
[113] K. Sahoo, P. Sarkar, P. Robin Davis, Artificial neural networks for prediction of compressive strength of recycled aggregate concrete, in: International Conference on Environment, Agricultural and Civil Engineering (ICEACE-2016), 2016. London, UK.
[114] G. Kalra, V. Pratyksh, J. Ebin, Research review and modeling of concrete compressive strength using artificial neural networks, Int. J. Innov. Sci. Eng. Technol. 3 (2) (2016) 672–677.
[115] M. Mirrashid, H. Naderpour, Recent trends in prediction of concrete elements behavior using soft computing (2010–2020), Arch. Comput. Methods Eng. 28 (4) (2021) 3307–3327.
[116] R. Gayathri, S.U. Rani, L. Čepová, M. Rajesh, K. Kalita, A comparative analysis of machine learning models in prediction of mortar compressive strength, Processes 10 (7) (2022) 1387.
[117] M.A. Haque, B. Chen, M.F. Javed, F.E. Jalal, Evaluating the mechanical strength prediction performances of fly ash-based MPC mortar with artificial intelligence approaches, J. Clean. Prod. 355 (2022) 131815.